

Landau Levels of the Euler Class Topology

Guan Yifei^{1,*}, Adrien Bouhon^{2,*}, and Oleg V. Yazyev^{1,3}

¹*Institute of Physics, École Polytechnique Fédérale de Lausanne (EPFL), CH-1015 Lausanne, Switzerland*

²*Nordic Institute for Theoretical Physics (NORDITA), Stockholm, Sweden and*

³*National Centre for Computational Design and Discovery of Novel Materials MARVEL, École Polytechnique Fédérale de Lausanne (EPFL), CH-1015 Lausanne, Switzerland*

(Dated: October 5, 2021)

Two-dimensional systems with $C_2\mathcal{T}$ (PT) symmetry exhibit the Euler class topology $E \in \mathbb{N}$ in each two-band subspace realizing a fragile topology beyond the symmetry indicators. By systematically studying the energy levels of Euler insulating phases in the presence of an external magnetic field, we reveal the robust gaplessness of the Hofstadter butterfly spectrum in the flat-band limit, while for the dispersive bands the gapping of the Landau levels is controlled by a hidden symmetry. We also find that the Euler class E of a two-band subspace gives a lower bound for the Chern numbers of the magnetic subgaps. Our study provides new fundamental insights into the fragile topology of flat-band systems going beyond the special case of $E = 1$ as e.g. in twisted bilayer graphene, thus opening the way to a very rich, still mainly unexplored, topological landscape with higher Euler classes.

Since the discovery of the integer quantum Hall effect (QHE) [1, 2] the concept of topology has played an increasing role in condensed matter physics [3–9]. The prediction of the quantum spin-Hall effect [10–13] and the three dimensional topological insulators (TI) [14–16] protected by time reversal symmetry have then opened the way to the realization of many novel electronic states and has attracted much attention to the topological aspects of electronic band structures. The role of symmetries has proven essential for the tenfold classification of topological phases of matter [17, 18] and its extension to crystalline symmetries [19–29]. This has recently culminated in systematic classification schemes that address the global band structure topology [30] in terms of irreducible representation combinatorics [31–33], symmetry-based indicators [34], the topological quantum chemistry [35, 36], and the real-space topological crystals [37–40]. The discrepancy between the stable symmetry indicators and the topology of split elementary band representations has then led to the definition of crystalline fragile topology for few-band subspaces [41–46].

In its most intriguing form, the fragile topology arises without symmetry indicators and is protected by an anti-unitary symmetry that squares to $+1$ and leaves the momentum invariant, e.g. PT symmetry in spinless systems, or $C_2\mathcal{T}$ symmetry in two-dimensional spinless and spinful materials, in which case it is called the Euler class topology [47–50]. Two-dimensional Euler insulating phases have been found to exhibit very rich physics, such as non-Abelian braiding of nodal points in electronic band structures [43, 48, 51], acoustic metamaterials [52] and in phonon band structures of silicates [53]. Furthermore, the Euler class topology has been found at the origin of Hopf linking signatures in quenched optical lattices [54], and the topology in magic-angle twisted bilayer graphene (TBG) [44, 55, 56].

The unveiling of further robust physical signatures for the Euler class topology is very timely. Recently, the effect of an external magnetic field on effective models of the moiré flat bands in TBG has been reported [57], as well as in other twisted bilayer systems [58]. By facilitating much higher magnetic flux per unit cell, moiré superlattices represent a great venue for the measurement of the Hofstadter butterfly spectrum [59, 60] as shown in [61, 62]. Reversely, the effect of different band structure topologies on the Hofstadter spectrum has been shown to lead to rich distinctive features [63].

In this work, we study the effect of the Euler class topology on the Hofstadter spectrum of two-dimensional systems. We reveal qualitative signatures of the Euler class in the flat-band limit and in more general non-degenerate and non-flat band structures. In particular, we provide the first systematic study of balanced and imbalanced Euler topological phases, which are characterized by equal, and, respectively, distinct Euler classes below and above the energy gap. While the flat-band limit exhibits robust gapless Hofstadter spectrum, we unveil a hidden symmetry that controls the gaplessness of the Hofstadter spectrum of the dispersive balanced Euler insulators. We furthermore show that the Hofstadter spectrum of the imbalanced phases is generically gapless.

Euler class topology.– The $C_{2z}\mathcal{T}$ symmetry of a two-dimensional system has $[C_{2z}\mathcal{T}]^2 = +1$ and leaves the momentum of the Bloch states invariant within the basal plane. This guarantees the existence of a basis with a real and symmetric Bloch Hamiltonian, $H \rightarrow \tilde{H} = \tilde{H}^T \in \mathbb{R}^N \times \mathbb{R}^N$ [48]. The Euler class $E \in \mathbb{Z}$ of real oriented rank-2 vector bundles [64] then characterizes the two-dimensional topology of every orientable [65] two-band subspace V^α of the band structure, which we label by $\alpha = I, II, \dots$, i.e. $V^\alpha = \langle u_a^\alpha, u_b^\alpha \rangle_{\mathbb{R}^2}$ with $\tilde{H}u_n^\alpha = \epsilon_n^\alpha u_n^\alpha$ and $\epsilon_n^\alpha < \epsilon_n^{\alpha+I}$ ($n = a, b$), while the topology for more bands

is characterized by the second Stiefel-Whitney class $w_2 \in \mathbb{Z}_2$ [43, 47–50]. The Euler class of the α -th orientable two-band subspace is computed through [43, 47, 48, 50, 66] $E_\alpha = 1/(2\pi) \int_{\text{BZ}} dk_1 dk_2 \text{Eu}_\alpha$ with $\text{BZ}=[-\pi, \pi]^2$ the Brillouin zone of a two-dimensional lattice, and the Euler curvature Eu_α is defined as the Pfaffian of the two-band Berry curvature $F[(u_a^\alpha, u_b^\alpha)]$ [67]

$$\begin{aligned} \text{Eu}_\alpha &= \text{Pf}F[(u_a^\alpha, u_b^\alpha)], \\ &= (\partial_{k_1} u_a^\alpha)^T \cdot (\partial_{k_2} u_b^\alpha) - (\partial_{k_2} u_a^\alpha)^T \cdot (\partial_{k_1} u_b^\alpha). \end{aligned} \quad (1)$$

Alternatively, the Euler class can be obtained as the winding of the two-band Wilson loop [42, 43, 47, 48, 66], see Fig. 1. Interestingly, Eq. (1) motivates yet another way to compute the Euler class. Defining the *Chern basis*

$$\begin{aligned} v_+^\alpha &= (u_a^\alpha + iu_b^\alpha)/\sqrt{2}, \\ v_-^\alpha &= (u_a^\alpha - iu_b^\alpha)/\sqrt{2}, \end{aligned} \quad (2)$$

we readily find $\text{Eu}_\alpha = F[v_+^\alpha]$ [68], from which we obtain [48] the Euler class as a Chern number $E_\alpha = |1/(2\pi) \int_{\text{BZ}} dk_1 dk_2 F[v_+^\alpha]| = |C|$. In the limit of degenerate bands ($\epsilon_a^\alpha = \epsilon_b^\alpha$), the Chern basis becomes an eigenbasis of \tilde{H} . This plays an important role in the flat-band limit discussed below. We also note an essential observable associated with the Euler class E_α , which is the number $2E_\alpha$ of *stable* nodal points hosted by the $\alpha(=I, II)$ -th two-band subspace, see *e.g.* the four stable nodes in Fig. 1(a). These nodes cannot be annihilated as long as the energy gaps above and below the two-band subspace remain open [43, 48, 49] [69].

Four-band real symmetric Hamiltonian.— In the following, we consider a four-orbital system that is insulating at half-filling ($\nu = N_{\text{occ}}/N_{\text{orb}} = 1/2$). The most general four-band real symmetric Bloch Hamiltonian is spanned by nine real independent terms, *i.e.* $\tilde{H} = \sum_{i,j=0,x,y,z} h_{ij} \Gamma_{ij}$ for $\Gamma_{ij} = \sigma_i \otimes \sigma_j$ and $i, j = 0, x, y, z$ with $\sigma_{x,y,z}$ the Pauli matrices and $\sigma_0 = \mathbb{1}$, under the reality constraint $\Im \Gamma_{ij} = 0$, such that only $\{h_{0x}, h_{0z}, h_{x0}, h_{xx}, h_{xz}, h_{yy}, h_{z0}, h_{zx}, h_{zz}\}$ are nonzero (not counting the term h_{00} that does not affect the topology).

We first consider the Hofstadter butterfly in the limit of flat bands. The flat-band limit of the Euler insulating phases implies the two-by-two degeneracy of the bands since each two-band subspace with a non-zero Euler class hosts stable nodal points. The Bloch Hamiltonian that is a homotopy representative for all the topological Euler insulating phases with eigenvalues $(\epsilon_1, \epsilon_2, \epsilon_3, \epsilon_4) = (-1, -1, 1, 1)$ eV is given by (see [70])

$$\begin{aligned} \tilde{H}[\mathbf{n}, \mathbf{n}'] &= n'_1 (n_1 \Gamma_{zz} + n_2 \Gamma_{zx} + n_3 \Gamma_{x0}) \\ &+ n'_2 (n_1 \Gamma_{xz} + n_2 \Gamma_{xx} + n_3 \Gamma_{z0}) \\ &+ n'_3 (n_1 \Gamma_{0x} + n_2 \Gamma_{0z} + n_3 \Gamma_{yy}), \end{aligned} \quad (3)$$

which is defined in terms of two unit vectors $\mathbf{n} = (\cos \phi \sin \theta, \sin \phi \sin \theta, \cos \theta)$ and $\mathbf{n}' =$

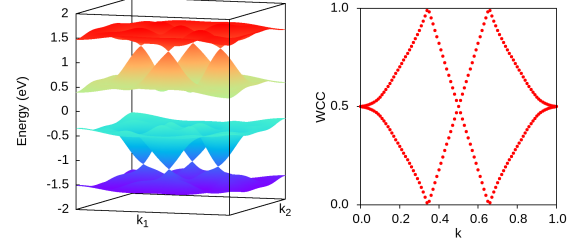


Figure 1. (a) Band structure of the tight-binding model of the balanced phase with the Euler class $E_I = E_{II} = 2$. Four nodal points are present in each two-band subspace as a consequence of the topology. (b) The value of the Euler class can be retrieved from the winding number 2 of the two-band Wilson loop.

$(\cos \phi' \sin \theta', \sin \phi' \sin \theta', \cos \theta')$. From the mapping of the Brillouin zone onto the unit spheres, $(k_1, k_2) \mapsto (\mathbf{n}, \mathbf{n}') \in (\mathbb{S}^2, \mathbb{S}^2)$, we obtain the tight-binding models [49]. Given the skyrmion number of one unit vector $W[\mathbf{n}] = 1/(2\pi) \int_{\text{BZ}} dk_1 dk_2 \mathbf{n} \cdot (\partial_{k_1} \mathbf{n} \times \partial_{k_2} \mathbf{n}) \in \mathbb{Z}$, the topology of Eq. (3) is determined by two skyrmion numbers, $q = W[\mathbf{n}]$ and $q' = W[\mathbf{n}']$, from which we obtain the Euler classes $E_I = |q - q'|$ and $E_{II} = |q + q'|$ [49] [70].

In this work we distinguish between two classes of phases: the *balanced* phases for which $E_I = E_{II}$, and the *imbalanced* phases with $E_I \neq E_{II}$. The balanced phases are readily obtained by setting one skyrmion number to zero, *e.g.* for $\mathbf{n}' = (0, 1, 0)$ we obtain $q' = 0$ and $E_I = E_{II} = |q|$, with the Hamiltonian $\tilde{H}_{\text{bal}}[\mathbf{n}] = \tilde{H}[\mathbf{n}, (0, 1, 0)] = n_1 \Gamma_{xz} + n_2 \Gamma_{xx} + n_3 \Gamma_{z0}$. The imbalanced phases are realized when both skyrmion numbers q and q' are nonzero, such that the nine terms in Eq. (3) are nonzero. Limiting ourselves to $E_I + E_{II} \leq 4$, we discuss the balanced phases for $(E_I, E_{II}) = (1, 1), (2, 2)$, and the imbalanced phases for $(E_I, E_{II}) = (0, 2), (1, 3)$, see Fig. 1 for the band structure and the Wilson loop of the balanced phase $(E_I, E_{II}) = (2, 2)$ (other phases are available in [70]).

Hofstadter Spectrum.— The effect of an external magnetic field $\mathbf{B} = \nabla \times \mathbf{A}$ is most conveniently introduced through the Peierls substitution $t_{ij} \rightarrow \tilde{t}_{ij} = t_{ij} \exp(i\phi_{ij})$ with $\phi_{ij} \propto \int_{\mathbf{R}_i}^{\mathbf{R}_j} \mathbf{A} \cdot d\mathbf{r}$ [71]. Restricting to a rational magnetic flux, *i.e.* $\phi = \int_{\text{u.c.}} B d^2\mathbf{r} = 2(r/s)\phi_0$ with r and s coprime integers ($\phi_0 = h/e$ is the magnetic flux quantum), the magnetic tight-binding Hamiltonian acquires a reduced periodicity with a magnetic unit cell [63] that is s times as large as the non-magnetic one [70]. It follows that the rotation C_{2z} acts as a nontrivial permutation of the s sub-lattice sites of the magnetic unit cell, leading to the breaking of $C_{2z}\mathcal{T}$ symmetry [72]. As a consequence, the $2E_\alpha$ nodal points of the α -th two-band subspace are

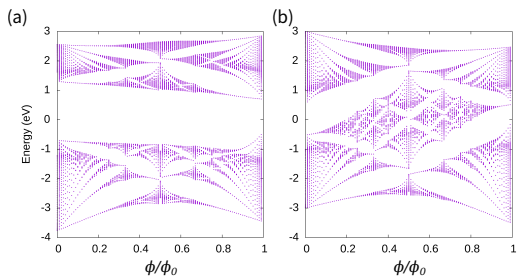


Figure 2. Hofstadter butterfly plots for (a) trivial and (b) topological Chern insulators. The Chern gap reaches the band edge as predicted by the Streda formula.

gapped by the magnetic field leading to magnetic Chern bands. The question is whether there are qualitative features of the Hofstadter spectrum that relate to the finite Euler classes E_I, E_{II} of the phases at zero field. [73]

Flat-band limit.— In the limit of small flux, the effect of an external magnetic field B on the energy levels takes the semi-classical form [74–77]

$$\epsilon_{n,B}(k) \approx \epsilon_{n,0}(k) + m_n(k) B, \quad (4)$$

where $\epsilon_{n,0}(k)$ is the energy eigenvalue at zero flux, and $m_n(k)$ describes the orbital magnetic susceptibility of the n -th band. In the case of the flat bands in TBG, $m_n(k)$ is related to the band topology [62]. The flatness of the bands minimizes the effect of dispersion and thus makes the Landau levels a good probe of quantum geometry [78], as the band topology induces a lower bound on the quantum metric.

While the phase with trivial topology ($E_I = E_{II} = 0$) is gapped, see Fig. 2(a), the nontrivial Euler phases are gapless with the Landau levels crossing at half-filling ($\nu = 1/2$) at a finite magnetic flux. Figure 3 shows the Hofstadter butterfly spectrum for different Euler phases in the flat-band limit. We find the qualitative trend that the Landau-level crossings at half-filling move toward zero for higher Euler classes, *i.e.* the least magnetic field at which the Landau levels cross, ϕ_{cross} , decreases with an increasing Euler class.

We now give the rationale for the gap-closing of the Hofstadter butterfly. Starting with the balanced phases, Fig. 3(a,b), we show in [70] that every $C_{2z}\mathcal{T}$ -symmetric Bloch Hamiltonian with degenerate bands is necessarily symmetric under an effective basal mirror symmetry $m_z = C_{2z}I$, with I the inversion symmetry and C_{2z} a spinful π -rotation (*i.e.* $C_{2z}^2 = -1$) [79]. We also find that the Chern basis Eq. (2), *i.e.* an eigenbasis of the balanced Hamiltonian in the flat-band limit, is an eigenbasis of the m_z symmetry operator [70]. There is thus a one-to-one correspondence between the signed Euler class and the mirror Chern number of the occupied bands, that is [70]

$$E_I^{(-i)} = C^{(-i)} = -C^{(i)} \in \mathbb{Z}, \quad (5)$$

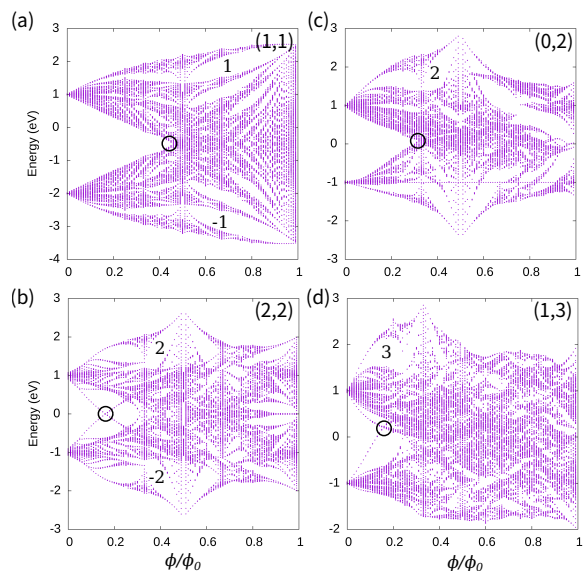


Figure 3. Hofstadter butterfly spectra calculated in the flat-band limit for the balanced phases with Euler classes (E_I, E_{II}) of (a) (1,1), (b) (2,2) and the imbalanced phases with (E_I, E_{II}) of (c) (0,2) and (d) (1,3).

where we have chosen the $(-i)$ mirror eigenvalue sector as a reference [80]. Given that m_z -symmetry is preserved at finite magnetic field B_z , the crossings between Landau levels of distinct mirror eigenvalues are protected by symmetry. We now can derive the qualitative trend as a function of the Euler class from the Streda formula $\nu = C^{(\mp i)}\phi/2 + \nu_0$ with $\nu_0 = 1/2$ the filling at zero flux [60]. Indeed, the subband with Chern number $C^{(\mp i)}$ must reach the band edge ($\nu = 0, 1$) at $\phi = 1/|C^{(\mp i)}|$, which gives an upper bound for the gap-closing flux in each m_z sector [81] (see Fig. 2(b) showing the Hofstadter spectrum of a generic Chern insulating phase with $C = +1$). We thus conclude that Landau levels of distinct m_z -eigenvalues must cross at half-filling (see also [63]), and through Eq. (5), with the trend of a smaller gap-closing flux for a higher Euler class, in agreement with the numerical results.

We now consider the imbalanced phases ($E_I \neq E_{II}$) in the flat-band limit, Fig. 3(c,d), where the same trend is observed. Contrary to the balanced case, there is no effective mirror symmetry [82], which leaves unexplained the stability of the Landau level crossing at half-filling [Fig. 3(c,d)]. Nevertheless, by making use of the Chern basis Eq. (2) as the eigenbasis, we can still decompose the bands at zero magnetic field into two decoupled imbalanced Chern insulators, *i.e.* $H = H^+ \oplus H^-$ with $C_I^\pm = \pm E_I$ and $C_{II}^\pm = \mp E_{II}$. The stability of the gaplessness of the Hofstadter spectrum, Fig. 3(c,d), suggests that the effect of the magnetic field introduced via the Peierls substitution preserves the decoupling between the two Chern sectors, even though there is no global symmetry of the Hamiltonian protecting the decoupling (like

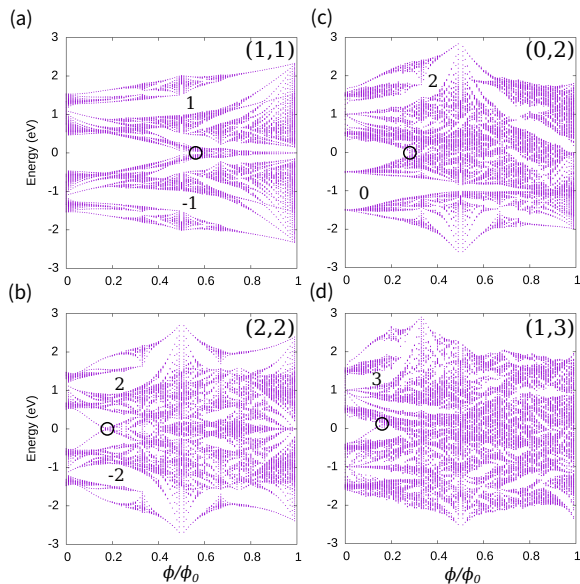


Figure 4. Hofstadter butterfly spectra calculated for the Euler insulating phases away from the flat-band and degenerate limit for Euler classes (a) (1,1), (b) (2,2), (c) (0,2) and (d) (1,3). While the effective m_z -symmetry is broken, the balanced phases all satisfy the hidden symmetry (see text). The magnetic subgap Chern numbers are bounded from below by the Euler classes.

m_z in the balanced case).

Dispersive bands.— We are now ready to address the more general situation of dispersive and non-degenerate Euler insulating phases [e.g. Fig. 1(a)]. Any adiabatic perturbation of Eq. (3) removes the degeneracy and the flatness of the bands, while preserving the Euler class topology. From the Hofstadter spectra shown in Fig. 4, we readily find that the gaplessness at half-filling remains a feature of the nontrivial Euler insulating phases, both for the balanced Fig. 4(a,b) and imbalanced Fig. 4(c,d) phases. This is somehow surprising since neither do the non-degenerate balanced phases preserve the effective m_z -symmetry (*i.e.* there is no mirror Chern number), nor does the Chern basis [Eq. (2)] gives eigenvectors of the Hamiltonian. We thus conclude that in principle nothing protects the unavoided crossing of Landau level branches across the gap of the Hofstadter spectra for the phases with nonzero Euler classes at zero flux, as was reported in Ref. [63] for the $E_I = E_{II} = 1$ case.

We resolve this apparent contradiction in the case of the balanced phases. Indeed, by systematically probing all perturbations of the Euler insulating phases allowed by $C_{2z}\mathcal{T}$ symmetry, we find that only the term h_{yy} added to $\tilde{H}_{\text{bal}}[\mathbf{n}] = \tilde{H}[\mathbf{n}, (0, 1, 0)]$ controls the gapping of the Hofstadter spectrum [70], see Fig. 5(a,b) obtained with a constant term $h_{yy} = \delta > 0$ added adiabatically. Since there is no global symmetry that can account for the vanishing or non-vanishing of this term, we call the condition $h_{yy} = 0$ a hidden symmetry of the balanced Euler

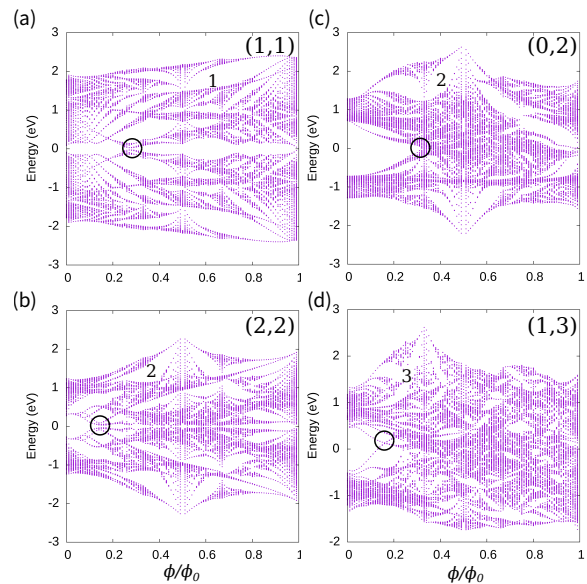


Figure 5. Effect of breaking the hidden symmetry on the Hofstadter butterfly spectra for balanced (a) (1,1), (b) (2,2) and imbalanced (c) (0,2), (d) (1,3) phases. The imbalanced phases remain gapless. The magnetic subgap Chern numbers are still bounded from below by the Euler classes.

insulating phases described by $\tilde{H}_{\text{bal}}[\mathbf{n}]$ [83]. We emphasize that the balanced Euler phases at zero flux shown in Fig. 4(a,b) all satisfy the hidden symmetry, *i.e.* all the terms $\{h_{ij}\}$ are non-zero except h_{yy} .

The imbalanced phases on the contrary are mainly unaffected by $C_{2z}\mathcal{T}$ -preserving perturbations, exhibiting a robust gapless Hofstadter spectrum, as one can see in Fig. 5(d-f) also obtained with $h_{yy} \neq 0$. This can be understood by noting that the flat degenerate imbalanced Bloch Hamiltonian, Eq. (3) with $q, q' \neq 0$, already has all nine independent terms $\{h_{ij}\}$ nonzero and without relations between them, such that a further perturbation in h_{yy} cannot lead to a qualitative change.

Landau levels and Chern numbers near the nodal points.— When the nodal points are well separated in energy from the rest of the bands, we can easily identify the Landau levels originating from the nodes at a small magnetic flux, *i.e.* at quarter fillings $\nu = 1/4 \pm 0^+, 3/4 \pm 0^+$ [see Fig. 4]. We find that the number of stable nodal points contained in each two-band subspace gives a lower bound for the Chern numbers of the subgaps above and below these Landau levels, *i.e.* $2E_\alpha \leq |C_{\nu=(2n+1)/4}|$. Indeed, the Chern numbers of the subgaps can be increased by adding unstable nodes, as e.g. in graphene.

Discussion.— We briefly discuss the difference between the Landau levels in Euler insulators and mirror Chern insulators or time reversal symmetric topological insulators. First of all, the \mathbb{N} Euler insulators are different from m_z insulators by the fragility [41–43, 57]. Despite the coincidence in flat two-band subspaces, m_z invariants are

preserved under the addition of trivial bands, contrary to the Euler class that falls into the \mathbb{Z}_2 second Stiefel-Whitney class in more than two bands. On the other hand, the \mathbb{Z}_2 Stiefel-Whitney insulators are also distinct from the Kane-Mele \mathbb{Z}_2 phases. As to the Hofstadter spectrum, the Kane-Mele invariant is protected by time reversal symmetry which is exactly broken by the magnetic field. In this case, if no other symmetry is present, the branch crossing is not protected [63].

We now discuss the potential candidates for observing the manifestations of Euler topology in the Hofstadter spectrum. Since the Landau levels rely on the effect of the magnetic field, our findings can be more naturally realized in electronic systems than in charge neutral systems, such as optical lattices [54] or acoustic metamaterials [52]. In that sense, the family of materials with moiré superlattices would be of interest. Indeed, Moiré superlattices in twisted heterostructures provide the possibility to realize and tune the fragile topology, while the large supercell facilitates the measurement of the Hofstadter butterfly that requires a very high magnetic flux per unit cell. We for instance propose the $M+N$ twisted multilayer graphene built by stacking the M -layer and N -layer graphene multilayers with a twist as a platform for realizing Euler insulators with arbitrary topological charge, since in such superlattices the flat bands can carry $(M-N)$ Chern numbers [84, 85].

We have studied the response of $C_2\mathcal{T}$ fragile topological insulators to external magnetic fields with tight-binding models hosting a variety of balanced and imbalanced Euler insulating phases. We have shown that the Hofstadter energy spectrum is affected qualitatively by the topological Euler class, especially in the flat-band limit. Our results also provide an insight for the study of topological flat-band systems with non-trivial quantum metric, such as the topologically bounded superfluid weight in twisted multilayered systems [66], generalizing to the very rich, yet mainly unexplored, landscape of phases with higher Euler classes.

Acknowledgement-Y.G. acknowledges support by the Swiss NSF (grant No. 172543) Computations were performed at the Swiss National Supercomputing Centre (CSCS) under projects Nos. s832 and s1008 and the facilities of Scientific IT and Application Support Center of EPFL.

* Contributed equally. Correspondence to yifei.guan@epfl.ch and adrien.bouhon@su.se.

- [1] K. v. Klitzing, G. Dorda, and M. Pepper, *Phys. Rev. Lett.* **45**, 494 (1980).
- [2] K. von Klitzing, *Rev. Mod. Phys.* **58**, 519 (1986).
- [3] R. B. Laughlin, *Phys. Rev. B* **23**, 5632 (1981).
- [4] D. J. Thouless, M. Kohmoto, M. P. Nightingale, and M. Den Nijs, *Phys. Rev. Lett.* **49**, 405 (1982).
- [5] M. Stone, ed., *Quantum hall effect* (World Scientific, Singapore, 1992).
- [6] D. Thouless, *Topological quantum numbers in nonrelativistic physics* (World Scientific, River Edge, 1998).
- [7] J. E. Avron, R. Seiler, and B. Simon, *Phys. Rev. Lett.* **51**, 51 (1983).
- [8] J. E. Avron, L. Sadun, J. Segert, and B. Simon, *Comm. Math. Phys.* **124**, 595 (1989).
- [9] Y. Hatsugai, *Phys. Rev. Lett.* **71**, 3697 (1993).
- [10] C. L. Kane and E. J. Mele, *Phys. Rev. Lett.* **95**, 226801 (2005).
- [11] C. L. Kane and E. J. Mele, *Phys. Rev. Lett.* **95**, 146802 (2005).
- [12] B. A. Bernevig and S.-C. Zhang, *Phys. Rev. Lett.* **96**, 106802 (2006).
- [13] B. A. Bernevig, T. L. Hughes, and S.-C. Zhang, *Science* **314**, 1757 (2006).
- [14] L. Fu, C. L. Kane, and E. J. Mele, *Phys. Rev. Lett.* **98**, 106803 (2007).
- [15] Y. L. Chen, J. G. Analytis, J.-H. Chu, Z. K. Liu, S.-K. Mo, X. L. Qi, H. J. Zhang, D. H. Lu, X. Dai, Z. Fang, S. C. Zhang, I. R. Fisher, Z. Hussain, and Z.-X. Shen, *Science* **325**, 178 (2009).
- [16] X.-L. Qi and S.-C. Zhang, *Rev. Mod. Phys.* **83**, 1057 (2011).
- [17] A. P. Schnyder, S. Ryu, A. Furusaki, and A. W. W. Ludwig, *Phys. Rev. B* **78**, 195125 (2008).
- [18] A. Kitaev, *AIP Conf. Proc.* **1134**, 22 (2009).
- [19] L. Fu and C. L. Kane, *Phys. Rev. B* **76**, 045302 (2007).
- [20] A. M. Turner, Y. Zhang, R. S. K. Mong, and A. Vishwanath, *Phys. Rev. B* **85**, 165120 (2012).
- [21] L. Fu, *Phys. Rev. Lett.* **106**, 106802 (2011).
- [22] C. Fang, M. J. Gilbert, and B. A. Bernevig, *Phys. Rev. B* **86**, 115112 (2012).
- [23] R.-J. Slager, A. Mesaros, V. Juričić, and J. Zaanen, *Nature Physics* **9**, 98 (2013).
- [24] C.-K. Chiu, H. Yao, and S. Ryu, *Phys. Rev. B* **88**, 075142 (2013).
- [25] C.-K. Chiu and A. P. Schnyder, *Phys. Rev. B* **90**, 205136 (2014).
- [26] K. Shiozaki and M. Sato, *Phys. Rev. B* **90**, 165114 (2014).
- [27] A. Alexandradinata, Z. Wang, and B. A. Bernevig, *Phys. Rev. X* **6**, 021008 (2016).
- [28] C.-K. Chiu, J. C. Y. Teo, A. P. Schnyder, and S. Ryu, *Rev. Mod. Phys.* **88**, 035005 (2016).
- [29] E. Cornfeld and A. Chapman, *Phys. Rev. B* **99**, 075105 (2019).
- [30] H. Watanabe, H. C. Po, M. P. Zaletel, and A. Vishwanath, *Phys. Rev. Lett.* **117**, 096404 (2016).
- [31] J. Kruthoff, J. de Boer, J. van Wezel, C. L. Kane, and R.-J. Slager, *Phys. Rev. X* **7**, 041069 (2017).
- [32] A. Bouhon and A. M. Black-Schaffer, *Phys. Rev. B* **95**, 241101(R) (2017).
- [33] K. Shiozaki, M. Sato, and K. Gomi, *Phys. Rev. B* **95**, 235425 (2017).
- [34] H. C. Po, A. Vishwanath, and H. Watanabe, *Nature Communications* **8**, 50 (2017).
- [35] B. Bradlyn, L. Elcoro, J. Cano, M. G. Vergniory, Z. Wang, C. Felser, M. I. Aroyo, and B. A. Bernevig, *Nature* **547**, 298 (2017).
- [36] J. Höller and A. Alexandradinata, *Phys. Rev. B* **98**, 024310 (2018).
- [37] Z. Song, S.-J. Huang, Y. Qi, C. Fang, and M. Hermele, *Science Advances* **5** (2019).

- [38] Z. Song, C. Fang, and Y. Qi, *Nature Communications* **11**, 4197 (2020).
- [39] R. Thorngren and D. V. Else, *Phys. Rev. X* **8**, 011040 (2018).
- [40] K. Shiozaki, C. Z. Xiong, and K. Gomi, (2018), [arXiv:1810.00801](https://arxiv.org/abs/1810.00801).
- [41] H. C. Po, H. Watanabe, and A. Vishwanath, *Phys. Rev. Lett.* **121**, 126402 (2018).
- [42] A. Bouhon, A. M. Black-Schaffer, and R.-J. Slager, *Phys. Rev. B* **100**, 195135 (2019).
- [43] J. Ahn, S. Park, and B.-J. Yang, *Phys. Rev. X* **9**, 021013 (2019).
- [44] Z.-D. Song, L. Elcoro, Y.-F. Xu, N. Regnault, and B. A. Bernevig, *Phys. Rev. X* **10**, 031001 (2020).
- [45] V. Peri, Z.-D. Song, M. Serra-Garcia, P. Engeler, R. Queiroz, X. Huang, W. Deng, Z. Liu, B. A. Bernevig, and S. D. Huber, *Science* **367**, 797 (2020).
- [46] Z.-D. Song, L. Elcoro, and B. A. Bernevig, *Science* **367**, 794 (2020).
- [47] J. Ahn, D. Kim, Y. Kim, and B.-J. Yang, *Phys. Rev. Lett.* **121**, 106403 (2018).
- [48] A. Bouhon, Q. Wu, R.-J. Slager, H. Weng, O. V. Yazyev, and T. Bzdušek, *Nature Physics* **16**, 1137 (2020).
- [49] A. Bouhon, T. Bzdušek, and R.-J. Slager, *Phys. Rev. B* **102**, 115135 (2020).
- [50] Y. X. Zhao and Y. Lu, *Phys. Rev. Lett.* **118**, 056401 (2017).
- [51] Q. Wu, A. A. Soluyanov, and T. Bzdušek, *Science* **365**, 1273 (2019).
- [52] B. Jiang, A. Bouhon, Z.-K. Lin, X. Zhou, B. Hou, F. Li, R.-J. Slager, and J.-H. Jiang, (2021), [arXiv:2104.13397](https://arxiv.org/abs/2104.13397).
- [53] B. Peng, A. Bouhon, B. Monserrat, and R.-J. Slager, (2021), [arXiv:2105.08733](https://arxiv.org/abs/2105.08733).
- [54] F. N. Únal, A. Bouhon, and R.-J. Slager, *Phys. Rev. Lett.* **125**, 053601 (2020).
- [55] H. C. Po, L. Zou, T. Senthil, and A. Vishwanath, *Phys. Rev. B* **99**, 195455 (2019).
- [56] J. Liu, J. Liu, and X. Dai, *Phys. Rev. B* **99**, 155415 (2019).
- [57] B. Lian, F. Xie, and B. A. Bernevig, *Phys. Rev. B* **102**, 041402(R) (2020).
- [58] B. Lian, Z. Liu, Y. Zhang, and J. Wang, *Phys. Rev. Lett.* **124**, 126402 (2020).
- [59] C. R. Dean, L. Wang, P. Maher, C. Forsythe, F. Ghahari, Y. Gao, J. Katoch, M. Ishigami, P. Moon, M. Koshino, and others, *Nature* **497**, 598 (2013).
- [60] I. Dana, Y. Avron, and J. Zak, *Journal of Physics C: Solid State Physics* **18**, L679 (1985).
- [61] Y. Cao, V. Fatemi, A. Demir, S. Fang, S. L. Tomarken, J. Y. Luo, J. D. Sanchez-Yamagishi, K. Watanabe, T. Taniguchi, E. Kaxiras, and others, *Nature* **556**, 80 (2018).
- [62] Q. Wu, J. Liu, Y. Guan, and O. V. Yazyev, *Phys. Rev. Lett.* **126**, 056401 (2021).
- [63] J. Herzog-Arbeitman, Z.-D. Song, N. Regnault, and B. A. Bernevig, *Phys. Rev. Lett.* **125**, 236804 (2020).
- [64] A. Hatcher, *Vector bundles and k-Theory* (Unpublished, 2003).
- [65] We are here excluding non-orientable phases that are characterized by the presence of π -Berry phases along some non-contractible loops of the Brillouin zone [47, 49].
- [66] F. Xie, Z. Song, B. Lian, and B. A. Bernevig, *Phys. Rev. Lett.* **124**, 167002 (2020).
- [67] We define the Berry curvature of the α -th two-band subspace spanned by the two real Bloch eigenvectors $\{u_a^\alpha, u_b^\alpha\}$ as $iF[|\mathbf{u}_\alpha\rangle] = \langle \partial_{k_1} \mathbf{u}_\alpha | \partial_{k_2} \mathbf{u}_\alpha \rangle - \langle \partial_{k_2} \mathbf{u}_\alpha | \partial_{k_1} \mathbf{u}_\alpha \rangle$ with the matrix of the α -th eigenvectors $|\mathbf{u}_\alpha\rangle = (u_a^\alpha, u_b^\alpha)$.
- [68] We have $F[v_+^\alpha] = (\partial_{k_1} v_+^\alpha)^T \cdot (\partial_{k_2} v_+^\alpha) - (\partial_{k_2} v_+^\alpha)^T \cdot (\partial_{k_1} v_+^\alpha)$.
- [69] It must be contrasted for instance with the two nodes of graphene that can be annihilated upon breaking the C_2 crystal symmetry, while preserving $C_2\mathcal{T}$.
- [70] Supplementary material, see Supplementary Material for details.
- [71] M. Graf and P. Vogl, *Phys. Rev. B* **51**, 4940 (1995).
- [72] We emphasize that while C_2 is not a symmetry of the Hamiltonian, $C_2\mathcal{T}$ imposes the C_2 -symmetric spatial configuration of the atomic orbitals since \mathcal{T} has no effect on the position operator. In other words, any orbital φ_β located away from a C_2 center, say \mathbf{r}_β , must have a C_2 partner located at $C_2\mathbf{r}_\beta$.
- [73] The Hofstadter calculations, band structures and the Wilson loop calculations are performed with the open-source package WannierTools [86].
- [74] Y. Gao, S. A. Yang, and Q. Niu, *Phys. Rev. B* **91**, 214405 (2015).
- [75] J. Shi, G. Vignale, D. Xiao, and Q. Niu, *Phys. Rev. Lett.* **99**, 197202 (2007).
- [76] A. Alexandradinata and L. Glazman, *Phys. Rev. B* **97**, 144422 (2018).
- [77] C. Wang, W. Duan, L. Glazman, and A. Alexandradinata, *Phys. Rev. B* **100**, 014442 (2019).
- [78] J.-W. Rhim, K. Kim, and B.-J. Yang, *Nature* **584**, 59 (2020).
- [79] The degenerate system is thus symmetric under the magnetic point group $2'/m = \{E, m_z, C_{2z}\mathcal{T}, IT\}$, with $[C_{2z}\mathcal{T}]^2 = +1$ and $[IT]^2 = -1$. The IT symmetry implies Kramers degenerate bands at all momenta. We conclude that the degenerate limit exists for all balanced Euler insulating phases without the need of fine-tuning. In other words, the degeneracy of the bands is always associated with a symmetry of the Hamiltonian such that it is not accidental, see [70] for a detailed exposition.
- [80] Interestingly, the enrichment of $C_{2z}\mathcal{T}$ -symmetric phases with m_z symmetry implies that each two-band vector subbundle becomes oriented with the signed Euler class as topological invariant, *i.e.* $E_I^{(-i)} \in \mathbb{Z}$, by virtue of attaching a fixed orientation to each mirror-eigenvalue sector. See also SI[70].
- [81] More precisely, the occupied Landau levels at half-filling with a Chern number $C_v = \max\{C_I^{(-i)}, C_I^{(i)}\}$ at zero flux must reach the filling $\nu = C_v/2 + 1/2$ at the flux $\phi = 1$ (*e.g.* $\nu = 1$ if $C_v = 1$), while the conduction Landau levels at half-filling with a Chern number $C_c = \max\{C_{II}^{(-i)}, C_{II}^{(i)}\}$ at zero flux must reach the filling $\nu = -C_c/2 + 1/2$ (note the sign change for the conduction bands) at the flux $\phi = 1$ (*e.g.* $\nu = 0$ if $C_c = 1$). Furthermore, if $C_v = C_I^{(-i)} > 0$ ($C_v = C_I^{(i)} > 0$), then $C_c = C_{II}^{(i)} > 0$ ($C_c = C_{II}^{(-i)} > 0$), since $C_I^{(\mp i)} + C_{II}^{(\mp i)} = 0$.
- [82] This implies that the band degeneracy of the tight-binding models requires fine tuning. The exact degeneracy, similarly to the flat-band limit, requires infinite-range hopping terms. In practice, it can be achieved in very good numerical approximation by keeping hopping terms up to sufficiently far neighbors, see [70].
- [83] We note that a change of basis of $\tilde{H}_{\text{bal}}[\mathbf{r}]$ will also change accordingly the term that controls the hidden symmetry.
- [84] J. Liu, Z. Ma, J. Gao, and X. Dai, *Phys. Rev. X* **9**, 031021

- (2019).
- [85] S. Zhang, B. Xie, Q. Wu, J. Liu, and O. V. Yazyev, (2020), [arXiv:2012.11964](https://arxiv.org/abs/2012.11964) [[cond-mat.mes-hall](https://arxiv.org/abs/2012.11964)].
- [86] Q. Wu, S. Zhang, H.-F. Song, M. Troyer, and A. A. Soluyanov, *Computer Physics Communications* **224**, 405 (2018).
- [87] A. Bouhon, [3-band and 4-band real symmetric tight-binding models with arbitrary Euler class](https://github.com/abouhon/EulerClassTightBinding), GitHub (2020), publicly available Mathematica code, <https://github.com/abouhon/EulerClassTightBinding>.
- [88] A. Bouhon, to appear soon (2021).
- [89] Y. Jiang, Z. Dun, S. Moon, H. Zhou, M. Koshino, D. Smirnov, and Z. Jiang, *Nano Letters* **18**, 7726 (2018).
- [90] Z. Yan, R. Bi, H. Shen, L. Lu, S.-C. Zhang, and Z. Wang, *Phys. Rev. B* **96**, 041103 (2017).
- [91] C. Fang, H. Weng, X. Dai, and Z. Fang, *Chinese Physics B* **25**, 117106 (2016).
- [92] Y. Hasegawa and M. Kohmoto, *Phys. Rev. B* **88**, 125426 (2013).

LIST OF CONTENTS

A. The modeling of Euler insulating phases.	8
We review the geometric approach of Ref. [49, 87], the homotopy classification of the Euler insulating phases, and the construction of tight-binding Hamiltonian for all homotopy classes.	
B. From complex to real basis.	9
We derive the general form of a four-band tight-binding model with $C_{2z}\mathcal{T}$ symmetry, assuming two s -orbitals with both spin-1/2 components.	
C. Basal mirror symmetry and twofold-band degeneracy.	10
We derive the one-to-one correspondence between the signed Euler class of degenerate balanced phases and the mirror Chern number. We prove that the band-degeneracy in the balanced phases are always related to a global symmetry of the Hamiltonian, while the band-degeneracy of imbalanced phases always requires fine tuning.	
D. Hidden symmetry of the dispersive balanced phases.	13
We define the hidden symmetry for our models and for the QHS model given in [63].	
E. Dispersive band structures at zero field.	14
We show the band structures away from the flat-band limit and the two-band Wilson loops of all the four-band tight-binding models for which we have computed the Hofstadter spectrum.	
F. Further Hofstadter spectra for higher Euler classes.	14
We show the Hofstadter spectra for the balanced phase $E_I = E_{II} = 3$, and for the imbalanced phase $(E_I, E_{II}) = (2, 4)$.	
G. Chern numbers within the magnetic subgaps.	14
We show the Hofstadter spectra for finite systems with open boundary conditions, revealing the chiral edge states of the magnetic Chern phases at finite magnetic field.	
H. Magnetic Hamiltonian.	14
We briefly review the Peierls substitution for the tight-binding models, and then derive in details a three-band magnetic tight-binding model.	
I. Magnetic moment of the complex bands.	17
We discuss the orbital magnetization of the complexified basis of Euler insulators.	
J. Hofstadter butterfly for three-band tight-binding models.	17
We present the Wilson loops and Hofstadter spectrum of three-band Euler insulator models, for the Euler classes $E_I = 2, 4$, and 6.	
K. Peierls paths and the periodicity of Hofstadter butterfly.	18
We discuss the overall periodicity of Hofstadter butterfly as a function of the quantum flux, based on the tight-binding models and Peierls substitution.	

Appendix A: The modeling of Euler insulating phases

1. The geometric approach of Ref. [49, 87]

We here briefly review the construction of the homotopy representative Hamiltonian for the four-band Euler insulating phases at half-filling following Ref. [49, 87].

The spectral decomposition of the 4×4 real symmetric Hamiltonian \tilde{H} , *i.e.* $\tilde{H}u_n = \epsilon_n u_n$ with the eigenvalue ϵ_n and the eigenvector $u_n \in \mathbb{R}^4$ for $n = 1, \dots, 4$, gives $\tilde{H} = R \cdot D \cdot R^T$ with $R = (u_1 \ u_2 \ u_3 \ u_4) \in \text{SO}(4)$ the matrix of real eigenvectors and $D = \text{diag}(\epsilon_1, \epsilon_2, \epsilon_3, \epsilon_4)$ the matrix of energy eigenvalues. In the following we set $\epsilon_1 = \epsilon_2 = -\epsilon$ and $\epsilon_3 = \epsilon_4 = \epsilon > 0$.

From the spectral decomposition and the degeneracy of the energy levels, we readily have that \tilde{H} is invariant under any gauge transformation $R \rightarrow RG$ with $G = G_v \oplus G_c$ and $G_v, G_c \in \text{O}(2)$, such that $\det G = \det(G_v) \det(G_c) = 1$. Defining the corresponding left coset $[R] = \{RG | G \in \text{S}[\text{O}(2) \times \text{O}_2]\}$, we thus find that the Hamiltonian is an element of the real *unoriented* Grassmannian as $[R] \in \text{SO}(4)/\text{S}[\text{O}(2) \times \text{O}(2)] = \text{Gr}_{2,4}^{\mathbb{R}}$.

We are here excluding non-orientable phases characterized by π -Berry phases along the two non-contractible loops of the Brillouin zone. While the Hamiltonian defines an *orientable* vector bundle (see Appendix A 2 below) [49, 88], it is convenient to first seek an element of the real *oriented* Grassmannian $\widetilde{\text{Gr}}_{2,4}^{\mathbb{R}} = \text{SO}(4)/[\text{SO}(2) \times \text{SO}(2)]$ to construct the Hamiltonian. This allows us to take advantage of the diffeomorphism $\widetilde{\text{Gr}}_{2,4}^{\mathbb{R}} \cong \mathbb{S}^2 \times \mathbb{S}^2$. Starting from the explicit parametrization of R as an generic element of $\text{SO}(4)$, the reduction to the oriented Grassmannian is then carried out through the Plücker embedding permitting the representation of the Grassmannian as a 4-dimensional manifold subspace of a 6-dimensional vector space (the second exterior power of \mathbb{R}^4), *i.e.*

$$\iota : \widetilde{\text{Gr}}_{2,4}^{\mathbb{R}} \hookrightarrow \bigwedge^2(\mathbb{R}^4) : [R] \mapsto (\mathbf{n}_+, \mathbf{n}_-) \in \mathbb{S}_+^2 \times \mathbb{S}_-^2, \quad (\text{A1})$$

where

$$\mathbf{n}_{\pm}(\phi_{\pm}, \theta_{\pm}) = (\cos \phi_{\pm} \sin \theta_{\pm}, \sin \phi_{\pm} \sin \theta_{\pm}, \cos \theta_{\pm}), \quad (\text{A2})$$

are the unit vectors on the two unit spheres \mathbb{S}_{\pm}^2 living in two perpendicular 3-dimensional vector subspaces of $\bigwedge^2(\mathbb{R}^4)$. Since the second arrow in Eq. (A1) is a bijection, we write the representative of each coset $[R]$ as $R(\mathbf{n}_+, \mathbf{n}_-)$, and the Hamiltonian is readily given by

$$\begin{aligned} \tilde{H}[\mathbf{n}_+, \mathbf{n}_-] = \\ R(\mathbf{n}_+, \mathbf{n}_-) \cdot \begin{pmatrix} -\epsilon \mathbb{1} & 0 \\ 0 & \epsilon \mathbb{1} \end{pmatrix} \cdot R(\mathbf{n}_+, \mathbf{n}_-)^T. \end{aligned} \quad (\text{A3})$$

See the Mathematica code of Ref. [87] for the explicit expression of $R(\mathbf{n}_+, \mathbf{n}_-)$ as a function of the four spherical angles $(\phi_+, \theta_+, \phi_-, \theta_-)$. Defining

$$\begin{aligned} \mathbf{n} &= \mathbf{n}_+, \\ \mathbf{n}' &= \mathbf{n}_-(\phi_- + \pi/2, \theta_- + \pi/2), \end{aligned} \quad (\text{A4})$$

and writing the components $\mathbf{n}^{(i)} = (n_1^{(i)}, n_2^{(i)}, n_3^{(i)})$, we get [49, 87]

$$\begin{aligned} \tilde{H}[\mathbf{n}, \mathbf{n}'] &= n'_1 (n_1 \Gamma_{zz} + n_2 \Gamma_{zx} + n_3 \Gamma_{x0}) \\ &+ n'_2 (n_1 \Gamma_{xz} + n_2 \Gamma_{xx} + n_3 \Gamma_{z0}) \\ &+ n'_3 (n_1 \Gamma_{0x} + n_2 \Gamma_{0z} + n_3 \Gamma_{yy}), \end{aligned} \quad (\text{A5})$$

with $\Gamma_{ij} = \sigma_i \otimes \sigma_j$ and the Pauli matrices $\{\sigma_i\}_{i=x,y,z}$, and with $\sigma_0 = \mathbb{1}$.

a. Homotopy classification

Considering the unit vector \mathbf{n} as a mapping from a base sphere \mathbb{S}_0^2 to a target sphere \mathbb{S}^2 , *i.e.* $\mathbf{n} = \mathbf{n}(\phi(\phi_0, \theta_0), \theta(\phi_0, \theta_0))$, we define the skyrmion number

$$W[\mathbf{n}] = \frac{1}{4\pi} \int_{\mathbb{S}_0^2} d\phi_0 d\theta_0 \mathbf{n} \cdot (\partial_{\phi_0} \mathbf{n} \times \partial_{\theta_0} \mathbf{n}) \in \mathbb{Z}, \quad (\text{A6})$$

that counts the number of times \mathbf{n} wraps the target sphere \mathbb{S}^2 as we cover the base sphere \mathbb{S}_0^2 one time. By setting

$$\begin{aligned} \mathbf{n}_q &= (\cos(q\phi_0) \sin \theta_0, \sin(q\phi_0) \sin \theta_0, \cos \theta_0), \\ \mathbf{n}'_{q'} &= (\cos(q'\phi_0) \sin \theta_0, \sin(q'\phi_0) \sin \theta_0, \cos \theta_0), \end{aligned} \quad (\text{A7})$$

we readily obtain

$$W[\mathbf{n}_q] = q, \text{ and } W[\mathbf{n}'_{q'}] = q', \quad (\text{A8})$$

in terms of which the homotopy classification of $\tilde{H}[\mathbf{n}_q, \mathbf{n}'_{q'}]$ in Eq. (A5) is defined, since

$$\begin{aligned} \pi_2[\widetilde{\text{Gr}}_{2,4}^{\mathbb{R}}] &= \pi_2[\mathbb{S}^2 \times \mathbb{S}^2] = \pi_2[\mathbb{S}^2] \oplus \pi_2[\mathbb{S}^2] \\ &= \mathbb{Z} \oplus \mathbb{Z} \ni (q, q'). \end{aligned} \quad (\text{A9})$$

2. Topology of the Bloch Hamiltonian

So far, we have not specified the parameter base space of the Hamiltonian. Considering a two-dimensional crystalline system, we aim at a Bloch Hamiltonian $\tilde{H}(\mathbf{k})$ parametrized by a momentum vector $\mathbf{k} = (k_1, k_2)$ inside the Brillouin zone $[-\pi, \pi]^2 \cong \mathbb{T}^2$.

Preceding the previous construction by a projection of the Brillouin zone onto the base sphere \mathbb{S}_0 , *i.e.*

$$\mathbb{T}^2 \rightarrow \mathbb{S}_0^2 \rightarrow \mathbb{S}^2 \times \mathbb{S}^{2'} : \mathbf{k} \mapsto \mathbf{n}_0(\mathbf{k}) \mapsto (\mathbf{n}_q(\mathbf{k}), \mathbf{n}'_{q'}(\mathbf{k})), \quad (\text{A10})$$

we obtain an explicit parametrization of the Hamiltonian Eq. (A5) as a Bloch Hamiltonian for all the homotopy classes, *i.e.*

$$\tilde{H}[\mathbf{n}, \mathbf{n}'] \rightarrow \tilde{H}[\mathbf{n}_q(\mathbf{k}), \mathbf{n}'_{q'}(\mathbf{k})]. \quad (\text{A11})$$

Writing the Euler classes (see main text) of the occupied and unoccupied bands E_I and E_{II} , respectively, we obtain the homotopy classification of the two-dimensional *orientable* (excluding π -Berry phases) four-band Euler insulating phases through

$$E_I = |q - q'|, \quad E_{II} = |q + q'|. \quad (\text{A12})$$

We importantly note the reduction

$$(q, q') \in \mathbb{Z}^2 \rightarrow (E_I, E_{II}) \in \mathbb{N}^2, \quad (\text{A13})$$

which is due to the fact that the orientation of a Bloch Hamiltonian can be changed adiabatically, leading to a distinction between the *oriented* and the *orientable* topologies, see Ref. [49] and [88] for a detailed discussion. We also note the sum rule

$$E_I + E_{II} = 0 \pmod{2}, \quad (\text{A14})$$

which guarantees the cancellation of the second Stiefel-Whitney class, *i.e.* $w_{2,I} + w_{2,II} = 0 \pmod{2}$.

a. Balanced and imbalanced phases

The above homotopy classification allows us to distinguish two types of phases, the balanced phases with $E_I = E_{II}$, and the imbalanced phases with $E_I \neq E_{II}$. The balanced phases are characterized by having one zero skyrmion number, *i.e.* either $q = 0$ or $q' = 0$, while the imbalanced phases are characterized by having two nonzero skyrmion numbers, *i.e.* $|q|, |q'| > 0$.

In Appendix B and C, we rederive in detail the general form and the topology of the Bloch Hamiltonian for the balanced phases with degenerate bands by starting from a system with spinful basal mirror symmetry. Indeed, we prove in Appendix C1 that a balanced Euler insulating phase has degenerate bands if and only if it has a spinful basal mirror symmetry.

3. Tight-binding Hamiltonian

Once the homotopy representative Hamiltonian has been parametrized in terms of the points of the Brillouin zone, as in $\tilde{H}[\mathbf{n}_q(\mathbf{k}), \mathbf{n}'_{q'}(\mathbf{k})]$, we get a tight-binding Bloch Hamiltonian by expanding each term as a Fourier series, *i.e.*

$$\begin{aligned} \tilde{H}_{ab}[\mathbf{n}_q(\mathbf{k}), \mathbf{n}'_{q'}(\mathbf{k})] = & \sum_{l_x, l_y \in \mathbb{Z}} \left[a_{(l_x, l_y)}^{(ab)} \cos(l_x k_x + l_y k_y) \right. \\ & \left. + b_{(l_x, l_y)}^{(ab)} \sin(l_x k_x + l_y k_y) \right]. \quad (\text{A15}) \end{aligned}$$

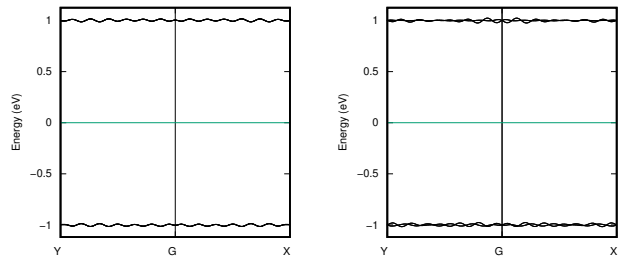


Figure 6. Band structures in the approximate flat-band limit for (a) the balanced phase $(E_I, E_{II}) = (2, 2)$, and (b) the imbalanced phase $(E_I, E_{II}) = (1, 3)$, obtained for $K = 12$ in Eq. (A15).

In practise, we only need to keep a finite number K of terms, such that $-K \leq l_x, l_y \leq K$, since the hopping parameters $\{a_{(l_x, l_y)}^{(ab)}, b_{(l_x, l_y)}^{(ab)}\}$ decrease rapidly with the distance $\sqrt{l_x^2 + l_y^2}$.

The explicit tight-binding models used in this work have been retrieved from Ref. [87] which provides a Mathematica notebook that generates four-band (and three-band) tight-binding models for arbitrary fixed Euler classes.

a. Flat-band limit

In our context, perfect flat bands would require to keep all hopping terms up to infinitely distant neighbors (*i.e.* $-\infty \leq l_{x,y} \leq \infty$ in Eq. (A15)). However, we obtain a very good numerical approximation of the flat bands by keeping hopping terms up to $K \approx 12$, see *e.g.* Fig. 6(a) and (b).

Appendix B: From complex to real basis

Usually, the tight-binding models of physical systems with $C_2\mathcal{T}$ -symmetry are not given in their real form. In order to fix ideas, let us start from the following Bloch-Löwdin orbital basis, composed of two s -orbitals located at the center of the unit cell, each taken with the two spin-1/2 components,

$$\begin{aligned} |\varphi, \mathbf{k}\rangle = & (|\varphi_{1,\uparrow}, \mathbf{k}\rangle |\varphi_{2,\uparrow}, \mathbf{k}\rangle |\varphi_{1,\downarrow}, \mathbf{k}\rangle |\varphi_{2,\downarrow}, \mathbf{k}\rangle), \\ = & \sum_{\mathbf{R}} e^{i\mathbf{k}\cdot\mathbf{R}} (|w_{1,\uparrow}, \mathbf{R}\rangle |w_{2,\uparrow}, \mathbf{R}\rangle |w_{1,\downarrow}, \mathbf{R}\rangle |w_{2,\downarrow}, \mathbf{R}\rangle), \quad (\text{B1}) \end{aligned}$$

where \mathbf{R} runs over all the Bravais vectors of the lattice, and $\langle \mathbf{r} | w_\alpha, \mathbf{R} \rangle = w_\alpha(\mathbf{r} - \mathbf{R})$ is the Wannier function of the orbital α localized at the lattice site \mathbf{R} . The Bloch Hamiltonian then reads,

$$\mathcal{H} = \sum_{\mathbf{k}} |\varphi, \mathbf{k}\rangle H(\mathbf{k}) \langle \varphi, \mathbf{k}|, \quad (\text{B2})$$

with

$$\begin{aligned} H(\mathbf{k}) &= \begin{pmatrix} H_{\uparrow\uparrow}(\mathbf{k}) & H_{\uparrow\downarrow}(\mathbf{k}) \\ H_{\downarrow\uparrow}(\mathbf{k}) & H_{\downarrow\downarrow}(\mathbf{k}) \end{pmatrix}, \\ &= \begin{pmatrix} H_{1\uparrow,1\uparrow}(\mathbf{k}) & H_{1\uparrow,2\uparrow}(\mathbf{k}) & H_{1\uparrow,1\downarrow}(\mathbf{k}) & H_{1\uparrow,2\downarrow}(\mathbf{k}) \\ H_{1\uparrow,2\uparrow}^*(\mathbf{k}) & H_{2\uparrow,2\uparrow}(\mathbf{k}) & H_{2\uparrow,1\downarrow}(\mathbf{k}) & H_{2\uparrow,2\downarrow}(\mathbf{k}) \\ H_{1\uparrow,1\downarrow}^*(\mathbf{k}) & H_{2\uparrow,1\downarrow}^*(\mathbf{k}) & H_{1\downarrow,1\downarrow}(\mathbf{k}) & H_{1\downarrow,2\downarrow}(\mathbf{k}) \\ H_{1\uparrow,2\downarrow}^*(\mathbf{k}) & H_{2\uparrow,2\downarrow}^*(\mathbf{k}) & H_{1\downarrow,2\downarrow}^*(\mathbf{k}) & H_{2\downarrow,2\downarrow}(\mathbf{k}) \end{pmatrix}, \end{aligned} \quad (\text{B3})$$

where we have imposed hermiticity.

Let us list the action on the Bloch orbital basis of a few symmetries that we use below,

$$\begin{aligned} C_{2z} |\varphi, \mathbf{k}\rangle &= |\varphi, C_{2z}\mathbf{k}\rangle (-i\sigma_z \otimes \mathbb{1}), \\ I |\varphi, \mathbf{k}\rangle &= |\varphi, -\mathbf{k}\rangle (\mathbb{1} \otimes \mathbb{1}), \\ m_z |\varphi, \mathbf{k}\rangle &= |\varphi, m_z \mathbf{k}\rangle (-i\sigma_z \otimes \mathbb{1}), \\ \mathcal{T} |\varphi, \mathbf{k}\rangle &= |\varphi, -\mathbf{k}\rangle (-i\sigma_y \otimes \mathbb{1}) \mathcal{K}, \\ C_{2z}\mathcal{T} |\varphi, \mathbf{k}\rangle &= |\varphi, m_z \mathbf{k}\rangle (i\sigma_x \otimes \mathbb{1}) \mathcal{K}, \\ I\mathcal{T} |\varphi, \mathbf{k}\rangle &= |\varphi, \mathbf{k}\rangle (-i\sigma_y \otimes \mathbb{1}) \mathcal{K}, \end{aligned} \quad (\text{B4})$$

where C_{2z} is the π rotation about the \hat{z} axis that is perpendicular to the basal plane containing the two-dimensional system, I is inversion, $m_z = C_{2z}I = IC_{2z}$ is the basal mirror, \mathcal{T} is time reversal, and \mathcal{K} is complex conjugation.

We now consider a system that is symmetric under $C_{2z}\mathcal{T}$ only, *i.e.* it must satisfy the constraint

$$(\sigma_x \otimes \mathbb{1}) H^*(m_z \mathbf{k}) (\sigma_x \otimes \mathbb{1}) = H(\mathbf{k}). \quad (\text{B5})$$

In 2D systems, the momenta belong to the m_z -invariant Brillouin zone, *i.e.* $m_z \mathbf{k} = \mathbf{k}$. As a consequence the blocks $H_{\sigma\sigma'}(\mathbf{k})$ that compose $H(\mathbf{k})$ must be of the form

$$\begin{aligned} H_{\uparrow\uparrow} &= H_1\sigma_x + H_2\sigma_y + H_3\sigma_z + H_4\mathbb{1}, \\ H_{\downarrow\downarrow} &= H_1\sigma_x - H_2\sigma_y + H_3\sigma_z + H_4\mathbb{1}, \\ H_{\uparrow\downarrow} &= \begin{pmatrix} H_5 + iH_6 & H_7 + iH_8 \\ H_7 + iH_8 & H_9 + iH_{10} \end{pmatrix}, \end{aligned} \quad (\text{B6})$$

where

$$\begin{aligned} H_1 &= \Re H_{1\uparrow,2\uparrow}, & H_6 &= \Im H_{1\uparrow,1\downarrow}, \\ H_2 &= -\Im H_{1\uparrow,2\uparrow}, & H_7 &= \Re H_{1\uparrow,2\downarrow}, \\ H_3 &= (H_{1\uparrow,1\uparrow} - H_{2\uparrow,2\uparrow})/2, & H_8 &= \Im H_{1\uparrow,2\downarrow}, \\ H_4 &= (H_{1\uparrow,1\uparrow} + H_{2\uparrow,2\uparrow})/2, & H_9 &= \Re H_{2\uparrow,2\downarrow}, \\ H_5 &= \Re H_{1\uparrow,1\downarrow}, & H_{10} &= \Im H_{2\uparrow,2\downarrow}, \end{aligned} \quad (\text{B7})$$

From $[C_{2z}\mathcal{T}]^2 = +1$ follows that there exists a basis in which $C_{2z}\mathcal{T}$ is represented by \mathcal{K} [48]. This basis is here

given by

$$\begin{aligned} |\tilde{\varphi}, \mathbf{k}\rangle &= |\varphi, \mathbf{k}\rangle \cdot V^\dagger, \\ V &= \sqrt{\sigma_x \otimes \mathbb{1}} \cdot \frac{1}{2} \begin{pmatrix} -1 & i & 1 & -i \\ i & -1 & i & -1 \\ -i & 1 & i & -1 \\ -1 & i & -1 & i \end{pmatrix}, \end{aligned} \quad (\text{B8})$$

for which

$$\begin{aligned} C_{2z}\mathcal{T} |\tilde{\varphi}, \mathbf{k}\rangle &= C_{2z}\mathcal{T} |\varphi, \mathbf{k}\rangle \cdot V^\dagger, \\ &= |\varphi, \mathbf{k}\rangle \cdot (i\sigma_x \otimes \mathbb{1}) V^T \mathcal{K}, \\ &= |\tilde{\varphi}, \mathbf{k}\rangle \cdot V (i\sigma_x \otimes \mathbb{1}) V^T \mathcal{K}, \\ &= |\tilde{\varphi}, \mathbf{k}\rangle \mathcal{K}. \end{aligned} \quad (\text{B9})$$

Rotating the Hamiltonian in the new basis, we define

$$\tilde{H}(\mathbf{k}) = V \cdot H(\mathbf{k}) \cdot V^\dagger, \quad (\text{B10})$$

that now must satisfy $\tilde{H}^*(\mathbf{k}) = \tilde{H}(\mathbf{k})$ as a consequence of $C_{2z}\mathcal{T}$ symmetry, *i.e.* $\tilde{H}(\mathbf{k})$ is real and symmetric.

In the “real” basis, the Hamiltonian thus has the generic form

$$\tilde{H} = \begin{pmatrix} h_{11} & h_{12} & h_{13} & h_{14} \\ h_{12} & h_{22} & h_{23} & h_{24} \\ h_{13} & h_{23} & h_{33} & h_{34} \\ h_{14} & h_{24} & h_{34} & h_{44} \end{pmatrix}, \quad (\text{B11})$$

where all elements h_{ij} are real and given by

$$\begin{aligned} h_{11} &= H_3 + H_4 - H_5, \\ h_{22} &= H_3 + H_4 + H_5, \\ h_{33} &= -H_3 + H_4 - H_9, \\ h_{44} &= -H_3 + H_4 + H_9, \\ h_{12} &= -H_6, \\ h_{13} &= -H_1 + H_7, \\ h_{14} &= H_2 - H_8, \\ h_{23} &= H_2 + H_8, \\ h_{24} &= H_1 + H_7, \\ h_{34} &= H_{10}. \end{aligned} \quad (\text{B12})$$

Appendix C: Basal mirror symmetry

Let us assume that the system satisfies the basal mirror symmetry m_z as well. Then, it must also have $-m_z C_{2z}\mathcal{T} = -C_{2z}^2 I\mathcal{T} = I\mathcal{T}$ symmetry. The system thus has the symmetries of the magnetic point group $2'/m = \{E, C_{2z}\mathcal{T}, m_z, I\mathcal{T}\}$. It readily follows that the off-diagonal blocks $H_{\uparrow\downarrow} = H_{\downarrow\uparrow}$ must vanish, *i.e.* $H_5 = H_6 = H_7 = H_8 = H_9 = H_{10} = 0$. The m_z -invariant Hamiltonian in the spinor basis then reads

$$H = H_{\uparrow\uparrow} \oplus H_{\downarrow\downarrow}. \quad (\text{C1})$$

Since $I\mathcal{T}\mathcal{H} = \mathcal{H}$ with $[I\mathcal{T}]^2 = -1$, the bands must be twofold-degenerate at all momenta, namely the bands are

Kramers degenerate. The eigenvalues are indeed readily found to be $\{E_o, E_o, E_u, E_u\}$, with

$$\begin{aligned} E_o &= H_4 - \epsilon, \quad E_u = H_4 + \epsilon, \\ \epsilon &= \sqrt{H_1^2 + H_2^2 + H_3^2}. \end{aligned} \quad (\text{C2})$$

We note that H_4 can be chosen arbitrarily without affecting the symmetry and the topology, we thus set $H_4 = 0$ without loss of generality. The eigenvectors are

$$\begin{aligned} v_o^{(\uparrow)} &= \begin{pmatrix} \sqrt{1-r^2} \\ -r e^{i\rho} \\ 0 \\ 0 \end{pmatrix}, \quad v_u^{(\uparrow)} = \begin{pmatrix} r \\ \sqrt{1-r^2} e^{i\rho} \\ 0 \\ 0 \end{pmatrix}, \\ v_o^{(\downarrow)} &= \begin{pmatrix} 0 \\ 0 \\ \sqrt{1-r^2} \\ -r e^{-i\rho} \end{pmatrix}, \quad v_u^{(\downarrow)} = \begin{pmatrix} 0 \\ 0 \\ r \\ \sqrt{1-r^2} e^{-i\rho} \end{pmatrix}, \end{aligned} \quad (\text{C3})$$

with

$$\rho = \text{Arg}\{H_1 + iH_2\}, \quad r^2 = \frac{\epsilon + H_3}{2\epsilon}. \quad (\text{C4})$$

The topology can now be directly assessed from a single spin sector, say from H_{\uparrow} . Imposing the condition of a band gap, *i.e.* $\epsilon > 0$, we define the unit vector

$$\mathbf{n} = \frac{1}{\epsilon}(H_1, H_2, H_3), \quad (\text{C5})$$

in terms of which we obtain the skyrmion number $W[\mathbf{n}]$ Eq. (A6). Since the H_{\downarrow} block is characterized by a unit vector $\mathbf{n}' = (H_1, -H_2, H_3)/\epsilon$, we have

$$W[\mathbf{n}'] = -W[\mathbf{n}]. \quad (\text{C6})$$

It can be checked that $W[\mathbf{n}]$ is identical to the Chern number computed through the surface integral of the Berry curvature of the occupied eigenvector, *i.e.*

$$\begin{aligned} F[v_o^{(\uparrow)}] &= -i \left[(\partial_{k_1} v_o^{(\uparrow)})^\dagger \cdot (\partial_{k_2} v_o^{(\uparrow)}) \right. \\ &\quad \left. - (\partial_{k_2} v_o^{(\uparrow)})^\dagger \cdot (\partial_{k_1} v_o^{(\uparrow)}) \right], \end{aligned} \quad (\text{C7})$$

which gives

$$C^{(\uparrow)} = \frac{1}{4\pi} \int d^2\mathbf{k} F[v_o^{(\uparrow)}] = W[\mathbf{n}], \quad (\text{C8})$$

and similarly

$$C^{(\downarrow)} = \frac{1}{4\pi} \int d^2\mathbf{k} F[v_o^{(\downarrow)}] = W[\mathbf{n}']. \quad (\text{C9})$$

Furthermore, since the m_z operator is diagonal in the orbital-spinor basis (see Eq. (B4)), we readily find the Chern number in the ($-i$)-mirror eigenvalue sector, *i.e.*

$$C^{(-i)} = C^{(\uparrow)} = W[\mathbf{n}], \quad (\text{C10})$$

called the mirror Chern number. Similarly, the mirror Chern number of the other sector is

$$C^{(i)} = C^{(\downarrow)} = W[\mathbf{n}'] = -W[\mathbf{n}]. \quad (\text{C11})$$

Moving to the real basis, we now show that there is a one-to-one correspondence between the mirror Chern number of one occupied mirror-polarized band and the signed Euler class of the occupied two-band subspace. First, let us write the m_z -invariant Hamiltonian in its real symmetric form,

$$\begin{aligned} \tilde{H} &= \begin{pmatrix} H_3 & 0 & -H_1 & H_2 \\ 0 & H_3 & H_2 & H_1 \\ -H_1 & H_2 & -H_3 & 0 \\ H_2 & H_1 & 0 & -H_3 \end{pmatrix}, \\ &= -H_1(\sigma_x \otimes \sigma_z) + H_2(\sigma_x \otimes \sigma_x) + 4H_3(\sigma_z \otimes \mathbb{1}). \end{aligned} \quad (\text{C12})$$

Assuming again the gap condition, *i.e.* $\epsilon^2 = H_1^2 + H_2^2 + H_3^2 > 0$, without loss of generality we can deform the Hamiltonian as $H_i \rightarrow n_i$ for $i = 1, 2, 3$, where (n_1, n_2, n_3) is the unit vector defined above. In other words, we can parametrize the Hamiltonian by the unit vector $\mathbf{n} = \mathbf{n}(\phi, \theta)$ with (ϕ, θ) the two angles of the unit sphere, through

$$\begin{aligned} H_1/\epsilon &= n_1 = \cos \phi \sin \theta, \\ H_2/\epsilon &= n_2 = \sin \phi \sin \theta, \\ H_3/\epsilon &= n_3 = \cos \theta. \end{aligned} \quad (\text{C13})$$

The eigenvalues are then $\{-1, -1, 1, 1\}$, and the two real eigenvectors of the occupied bands are given by

$$\begin{aligned} u_1(\phi, \theta) &= \sqrt{\cos(\theta/2)^2} \begin{pmatrix} \sin \phi \tan(\theta/2) \\ \cos \phi \tan(\theta/2) \\ 0 \\ -1 \end{pmatrix}, \\ u_2(\phi, \theta) &= \sqrt{\cos(\theta/2)^2} \begin{pmatrix} -\cos \phi \tan(\theta/2) \\ \sin \phi \tan(\theta/2) \\ -1 \\ 0 \end{pmatrix}. \end{aligned} \quad (\text{C14})$$

Then, the wedge product of the two occupied bands (which is motivated by the Plücker embedding [49]) gives

$$\begin{aligned} \begin{pmatrix} u_1^3 u_2^2 - u_1^2 u_2^3 \\ u_1^3 u_2^1 - u_1^1 u_2^3 \\ u_1^1 u_2^2 - u_1^2 u_2^1 \\ u_1^4 u_2^1 - u_1^1 u_2^4 \\ u_1^2 u_2^4 - u_1^4 u_2^2 \\ u_1^3 u_2^4 - u_1^4 u_2^3 \end{pmatrix} \cdot \begin{pmatrix} \mathbb{1}_3 & \mathbb{1}_3 \\ \mathbb{1}_3 & -\mathbb{1}_3 \end{pmatrix} &= \begin{pmatrix} \cos \phi \sin \theta \\ \sin \phi \sin \theta \\ -\cos \theta \\ 0 \\ 0 \\ 1 \end{pmatrix} \\ &= (n_1, n_2, -n_3, 0, 0, 1)^T. \end{aligned} \quad (\text{C15})$$

This explicitly shows that the signed Euler class of the two occupied bands is readily given by the (oriented) number of times $\mathbf{n}(\phi(k_x, k_y), \theta(k_x, k_y))$ wraps the sphere

when (k_x, k_y) covers the Brillouin zone one time [49]. In other words, through Eq. (C10) we find

$$E_I^{(-i)} = C^{(-i)} \in \mathbb{Z}. \quad (\text{C16})$$

A few comments are needed here. In general (*i.e.* without mirror symmetry), the sign of the Euler class is not uniquely defined because, as noted above, Hamiltonians only define *orientable* vector bundles (instead of *oriented* vector bundles) as a consequence of the gauge freedom $u_i \rightarrow \pm u_i$ for every eigenvector, which allows to flip the sign of the wedge product between the two occupied eigenvectors, *i.e.* $u_1 \wedge u_2 \rightarrow -u_1 \wedge u_2$. This has the consequence that there exist adiabatic transformations of the Hamiltonian that flip the sign of the Euler class, leading to the classification $(E_I, E_{II}) \in \mathbb{N}^2$ [49, 88]. Under the constraint of the basal mirror symmetry m_z though, one can associate a signed winding number to a fixed mirror eigenvalue sector.

Let us write the representation of m_z in the basis of real eigenvectors, *i.e.*

$$\begin{pmatrix} u_1^T \\ u_2^T \end{pmatrix} \cdot \tilde{U}_{m_z} \cdot (u_1 \ u_2) = \begin{pmatrix} 0 & 1 \\ -1 & 0 \end{pmatrix}, \quad (\text{C17})$$

where

$$\tilde{U}_{m_z} = V^\dagger \cdot (-i\sigma_z \otimes \mathbb{1}) \cdot V = \sigma_z \otimes i\sigma_y \quad (\text{C18})$$

is the representation of m_z in the “real” Bloch orbital basis Eq. (B8). The eigenbasis of m_z is thus given through the complexification (see the Chern basis in the main text)

$$\begin{aligned} v_+ &= (u_1 + iu_2)\sqrt{2}, \\ v_- &= (u_1 - iu_2)/\sqrt{2}, \end{aligned} \quad (\text{C19})$$

i.e.

$$\begin{pmatrix} v_+^\dagger \\ v_-^\dagger \end{pmatrix} \cdot \tilde{U}_{m_z} \cdot (v_+ \ v_-) = \begin{pmatrix} -i & 0 \\ 0 & i \end{pmatrix} = -i\sigma_z, \quad (\text{C20})$$

which is now diagonal, such that v_\pm are eigenvectors of m_z with the eigenvalues $\mp i$. (Note that we actually recover the action of m_z on the spinor basis given in Eq. (B4).) It is now transparent from Eq. (C20) that the relative sign between u_1 and u_2 , and thus the sign of the Euler class (fixed by the wedge product $u_1 \wedge u_2$), is fixed by the mirror symmetry, since the gauge transformation $u_1 \wedge u_2 \rightarrow -u_1 \wedge u_2$ implies $v_\pm \rightarrow v_\mp$ which is forbidden under the constraint of a fixed mirror-eigenvalue sector. Note that the gauge transformation $(u_1, u_2) \rightarrow (-u_1, -u_2)$ is allowed since it doesn’t change the fixed mirror-eigenvalue sector, nor does it change the signed Euler class.

We emphasise that $\{v_1, v_2\}$ are still eigenvectors of the Hamiltonian since the energy eigenvalues for u_1 and u_2 are degenerate. Furthermore, we readily recover the $(-i)$ -

and (i) -mirror Chern numbers as the Chern numbers of v_1 and v_2 , respectively. It is now apparent that the winding associated to a nontrivial Euler class in Eq. (C15), directly implies the winding associated to the mirror Chern numbers, according to Eq. (C10). We conclude that by imposing that $u_1 + iu_2$ has the mirror eigenvalue $-i$, there is a one-to-one correspondence between the signed Euler class $E_I^{(-i)}$ (Eq. (C15)) and the $(-i)$ -mirror Chern number $C^{(-i)}$ (Eq. (C10)), leading to Eq. (C16).

1. All degenerate balanced phases are mirror symmetric

Importantly, the above reasoning for balanced Euler insulating phases can be reversed. Namely, for every (orientable) balanced ($E_I = E_{II}$) topological phase with only the $C_{2z}\mathcal{T}$ symmetry, whenever we impose the two-by-two degeneracy of the bands, there must be an effective basal mirror symmetry m_z (spinful with $m_z^2 = -1$), leading to the effective IT symmetry with $[IT]^2 = -1$. In other words, the degeneracy of the bands is always associated with a symmetry of the Hamiltonian and no fine tuning is needed.

We prove this by going back to the general geometric form from which all our tight-binding Hamiltonian are derived, Eq. (A5). First of all, all Hamiltonian belonging to $\text{Gr}_{2,4}^{\mathbb{R}}$ can be adiabatically mapped to a twofold-degenerate Hamiltonian. By construction the representative of each (orientable) homotopy class $\tilde{H}[\mathbf{n}, \mathbf{n}']$ is twofold degenerate. Without loss of generality, the balanced phases are obtained by fixing \mathbf{n}' to be non-winding, *i.e.* $q' = W[\mathbf{n}'] = 0$. (We can equivalently fix \mathbf{n} and let \mathbf{n}' winds instead, since there is an adiabatic mapping from one parametrization to the other parametrization [88].) Let us fix $\mathbf{n}' = \bar{\mathbf{n}} = (0, 1, 0)$, we find that it is mirror symmetric with

$$\tilde{U}_{m_z} \cdot \tilde{H}[\mathbf{n}, \bar{\mathbf{n}}] \cdot \tilde{U}_{m_z}^T = \tilde{H}[\mathbf{n}, \bar{\mathbf{n}}], \quad (\text{C21})$$

where \tilde{U}_{m_z} is defined in Eq. (C18). Comparing $\tilde{H}[\mathbf{n}, \mathbf{n}']$ with two different fixed unit vector \mathbf{n}' , *i.e.* in one case $\mathbf{n}' = \bar{\mathbf{n}}$ and in the other case $\mathbf{n}' = \mathbf{n}_1 \neq \bar{\mathbf{n}}$, we find

$$\begin{aligned} \tilde{H}[\mathbf{n}, \bar{\mathbf{n}}] &= \\ &\Delta R[\mathbf{n}, \bar{\mathbf{n}}, \mathbf{n}_1] \cdot \tilde{H}[\mathbf{n}, \mathbf{n}_1] \cdot \Delta R[\mathbf{n}, \bar{\mathbf{n}}, \mathbf{n}_1]^T, \end{aligned} \quad (\text{C22})$$

with

$$\Delta R[\mathbf{n}, \bar{\mathbf{n}}, \mathbf{n}_1] = R[\mathbf{n}, \bar{\mathbf{n}}] \cdot R[\mathbf{n}, \mathbf{n}_1]^T. \quad (\text{C23})$$

Substituting Eq. (C22) in Eq. (C21), we then obtain

$$\Delta \tilde{U}_{m_z}(\mathbf{n}_1) \cdot \tilde{H}[\mathbf{n}, \mathbf{n}_1] \cdot \Delta \tilde{U}_{m_z}(\mathbf{n}_1)^T = \tilde{H}[\mathbf{n}, \mathbf{n}_1], \quad (\text{C24})$$

with

$$\begin{aligned} \Delta\tilde{U}_{m_z}(\mathbf{n}_1) &= \Delta R[\mathbf{n}, \bar{\mathbf{n}}, \mathbf{n}_1]^T \cdot \tilde{U}_{m_z} \cdot \Delta R[\mathbf{n}, \bar{\mathbf{n}}, \mathbf{n}_1], \\ &= \begin{pmatrix} 0 & c_{\phi_1}c_{\theta_1} & s_{\theta_1} & s_{\phi_1}c_{\theta_1} \\ -c_{\phi_1}c_{\theta_1} & 0 & -s_{\phi_1}c_{\theta_1} & s_{\theta_1} \\ -s_{\theta_1} & s_{\phi_1}c_{\theta_1} & 0 & -c_{\phi_1}c_{\theta_1} \\ -s_{\phi_1}c_{\theta_1} & -s_{\theta_1} & c_{\phi_1}c_{\theta_1} & 0 \end{pmatrix}, \end{aligned} \quad (\text{C25})$$

with $c_\beta = \cos \beta$ and $s_\beta = \sin \beta$ for $\beta = \phi_1, \theta_1$, *i.e.* the deformed Hamiltonian $\tilde{H}[\mathbf{n}, \bar{\mathbf{n}}] \rightarrow \tilde{H}[\mathbf{n}, \mathbf{n}_1]$ is still mirror symmetric, with a constant mirror operator $\Delta\tilde{U}_{m_z}(\mathbf{n}_1)$.

Interestingly, we can consider more general adiabatic transformations for which \mathbf{n}' is non-constant but still non-winding, *i.e.* $\mathbf{n}' = \mathbf{n}'(\mathbf{k})$. In that case, the “mirror” symmetry operator is non-constant as well with a nontrivial action of the “mirror” symmetry on the momentum. We will explore such phases elsewhere.

Since our homotopy representative Hamiltonian of the balanced Euler insulating phases covers all the balanced homotopy classes (with $q' = 0$ and $q \in \mathbb{Z}$), we conclude with the following statement: *Every (two-dimensional, four-band at half-filling, orientable) balanced Euler insulating phase is (spinful) mirror symmetric with respect to the basal plane if and only if the energy eigenvalues are twofold-degenerate.*

2. Degenerate imbalanced phases

Contrary to the balanced case, the imbalanced Euler insulating phases ($E_I \neq E_{II}$) with twofold-degenerate energy eigenvalues are never compatible with an effective mirror symmetry m_z , and thus there is no Kramers degeneracy. As a consequence, the degeneracy of the bands for these phases always requires fine tuning.

Let us prove this. The imbalanced condition imposes that $q, q' \neq 0$, *i.e.* the two unit vectors \mathbf{n} and \mathbf{n}' both wind. We simply define the imbalanced Hamiltonian from the balanced one through Eq. (C22), where we substitute the constant unit vector \mathbf{n}_1 to the winding one \mathbf{n}' . As a consequence, the degenerate imbalanced Hamiltonian satisfies Eq. (C24) but now with a mirror symmetry operator $\Delta\tilde{U}_{m_z}(\mathbf{n}')$ in Eq. (C25) that winds. Therefore, the condition Eq. (C24) cannot be interpreted as the symmetry of one fixed homotopy class. Since the degeneracy of the bands in one imbalanced homotopy class is never associated with a global symmetry of the Hamiltonian, it is accidental and can only be realized through fine tuning.

It can be verified with the Mathematica notebook of Ref. [87] that the degeneracy of the bands of imbalanced phases is never exact whenever we truncate the Fourier expansion of Eq. (A15). However, since the hopping parameters decay rapidly, similarly to the flat-band limit, we obtain degenerate bands in a good numerical approximation, see *e.g.* Fig. 6(b) showing the band structure of

the phase $(E_I, E_{II}) = (1, 3)$ obtained for $K = 12$ where both degeneracy and flatness have been imposed.

Appendix D: Hidden symmetry of the dispersive balanced phases and comparison with the QHS model

The non-degenerate phases break the mirror symmetry m_z . The constraint of the $C_{2z}\mathcal{T}$ symmetry alone allows all the terms of the real symmetric Hamiltonian in Eq. (B11) to be nonzero. Form the systematic probe of all allowed (adiabatic) perturbations of the model $\tilde{H}_{\text{bal}}[\mathbf{n}] = \tilde{H}[\mathbf{n}, (0, 1, 0)]$ given by Eq. (A5) (see also the main text), we have found that the gapping of the Hofstadter spectrum at half-filling only happens when $h_{14} \neq h_{23}$. Setting $h_{23} = h + \delta$ and $h_{14} = h - \delta$, a general (real symmetric) balanced Hamiltonian then takes the form

$$\tilde{H}_{\text{bal}} = \tilde{H}_{\text{bal}}[\delta = 0] + \delta(\sigma_y \otimes \sigma_y), \quad (\text{D1})$$

with $\delta = (h_{23} - h_{14})/2$.

We call the condition $\delta = 0$ a hidden symmetry of the balanced Hamiltonian at finite flux. In other words, every tight-binding Hamiltonian that is of the form $\tilde{H}_{\text{bal}}[\delta = 0]$ satisfies the hidden symmetry and exhibits a gapless Hofstadter spectrum. On the contrary, any model with $|\delta| > 0$ has a gapped Hofstadter spectrum.

a. Comparison with the QSH model

In Ref. [63] the authors have considered the BHZ model of the Quantum Spin Hall phase (QSH) and its generalization when only the $C_{2z}\mathcal{T}$ symmetry is preserved and restricting to balanced phases, which they call H'''_{QSH} . For exhaustiveness we give here the mapping from H'''_{QSH} (which is not in its real form) to our models in Eq. (B11).

We first write H'''_{QSH} in its generic form, *i.e.*

$$\begin{aligned} H'''_{QSH} &= a_0(\mathbb{1} \otimes \mathbb{1}) + a_1(\mathbb{1} \otimes \sigma_z) + a_2(\sigma_z \otimes \sigma_x) + \\ &a_3(\sigma_z \otimes \sigma_x) + a_4(\sigma_y \otimes \sigma_z) + a_5(\sigma_x \otimes \mathbb{1}) + a'_5(\sigma_y \otimes \mathbb{1}) + \\ &a_6(\sigma_x \otimes \sigma_y) + a'_6(\sigma_y \otimes \sigma_y) + a''_6(\sigma_x \otimes \sigma_z), \end{aligned} \quad (\text{D2})$$

where we have added the term $a_4(\sigma_y \otimes \sigma_z)$ which is allowed by $C_{2z}\mathcal{T}$ but not present in the model of Ref. [63]. (We note that we are not concerned here with the specific expressions of the terms of H'''_{QSH} given in Ref. [63] which realizes the phase $E_I = E_{II} = 1$.)

We now perform a change of basis that brings H'''_{QSH} in its real form in order to compare it with our models. We define

$$\tilde{H}'''_{QSH} = P \cdot V \cdot H'''_{QSH} \cdot V^\dagger \cdot P, \quad (\text{D3})$$

that is real and symmetric, with

$$V = \sqrt{\sigma_x \otimes \sigma_z}, \quad P = \begin{pmatrix} 1 & 0 & 0 & 0 \\ 0 & 0 & 1 & 0 \\ 0 & 1 & 0 & 0 \\ 0 & 0 & 0 & 1 \end{pmatrix}. \quad (\text{D4})$$

Writing it explicitly, we have

$$\tilde{H}_{QSH}''' = \begin{pmatrix} h_{11} & h_{12} & h_{13} & h_{14} \\ h_{12} & h_{22} & h_{23} & h_{24} \\ h_{13} & h_{23} & h_{33} & h_{34} \\ h_{14} & h_{24} & h_{34} & h_{44} \end{pmatrix}, \quad (\text{D5})$$

with

$$\begin{aligned} h_{11} &= a_0 + a_1 + a_4 + a'_5 \\ h_{22} &= a_0 + a_1 - a_4 - a'_5 \\ h_{33} &= a_0 - a_1 + a_4 - a'_5 \\ h_{44} &= a_0 - a_1 - a_4 + a'_5 \\ h_{12} &= a_5 + a''_6 \\ h_{13} &= a_2 - a_6 \\ h_{14} &= -a_3 - a'_6 \\ h_{23} &= -a_3 + a'_6, \\ h_{24} &= -a_2 - a_6, \\ h_{34} &= a_5 - a''_6. \end{aligned} \quad (\text{D6})$$

In agreement with our finding of the hidden symmetry, we have verified that only the nonzero term $a'_6(\sigma_y \otimes \sigma_y)$ of H_{QSH}''' leads to the gapping of the Hofstadter spectrum. We indeed have

$$a'_6 = \frac{h_{23} - h_{14}}{2} = \delta, \quad (\text{D7})$$

which is the term responsible for the hidden symmetry discussed above.

Appendix E: Dispersive band structures at zero field

We show in Fig. 7 the dispersive band structures and the unoccupied two-band Wilson loops of the tight-binding models for which we have computed the Hofstadter spectrum. Fig. 7(a-c) show the balanced phases, and Fig. 7(d-f) show the imbalanced phases. We have considered longer-range hoppings in the tight-binding models of the imbalanced phase, *i.e.* $K = 12$ in Eq. (A15), in order to obtain the nodal points well separated in energy from the rest of the bands.

Appendix F: Further Hofstadter spectra for higher Euler classes

We present here further results in Fig. 9 obtained with higher Euler classes: for the balanced phase with

$E_I = E_{II} = 3$, and for the imbalanced phase with $(E_I, E_{II}) = (2, 4)$. Similarly to the phases discussed in the main text, we find that the Hofstadter spectrum is gapless for the Euler phases in the flat-band limit [Fig. 9(a,b)] as well as for the dispersive phases satisfying the hidden symmetry ($h_{yy} = 0$) [Fig. 9(c,d)]. Then, while the dispersive balanced phase becomes gapped upon breaking the hidden symmetry [Fig. 9(e)], the imbalanced phases remain gapless [Fig. 9(f)].

Noticing that the Euler number is only valid in 2-band subspaces, we also present the case where an even Euler number is trivialized by adding an additional band to the occupied subspace. In 8, one of the trivial bands in $(E_I, E_{II}) = (2, 0)$ model is added into the occupied subspace. As a consequence, the Euler number is trivialized and gap-closing is then absent.

Appendix G: Chern numbers within the magnetic subgaps

Whenever a two-band subspace $\alpha (= I, II)$ is not degenerate, an Euler class E_α implies the presence of $2E_\alpha$ stable nodes. The stability of the nodes of a two-band subspace with a nonzero Euler class protected by $C_{2z}\mathcal{T}$ is more fundamentally understood from their non-Abelian topological charges. These originate from the multi-gap condition of the band structure [43, 48, 49, 88]. Graphene for instance has two nodal points with opposite non-Abelian charges (indicating that the nodes can be annihilated if we merge them upon breaking the hexagonal symmetry while keeping $C_{2z}\mathcal{T}$). The nodes of the Euler phases have additive (non-Abelian) topological charges, indicating their stability upon collision. It is thus very interesting to ask whether the non-Abelian charges of the nodes have any effect on the Hofstadter spectrum. One condition for such an observation is the well separation of the nodes in energy from the rest of the bands, like *e.g.* in graphene, which is the case in our models.

We find in the main text (and in Appendix F) that the nodal points are the origins of nearly flat Landau levels. This is reminiscent of the Landau levels associated to Weyl points [89–91].

We also show in the main text (and in Appendix F) that the Euler class E_α provides a lower bound for the Chern numbers of the magnetic subgaps, *i.e.* at $\nu = 1/4 \pm 0^+, 3/4 \pm 0^+$. We confirm this from the chiral edge states obtained for a geometry with open boundary condition at a small magnetic flux, see *e.g.* Fig. 10 for the phases $(E_I, E_{II}) = (1, 1)$ and $(3, 3)$.

Appendix H: Magnetic Hamiltonian

The effect of an external magnetic field $\mathbf{B} = \nabla \times \mathbf{A}$ is most conveniently captured through the Peierls substitu-

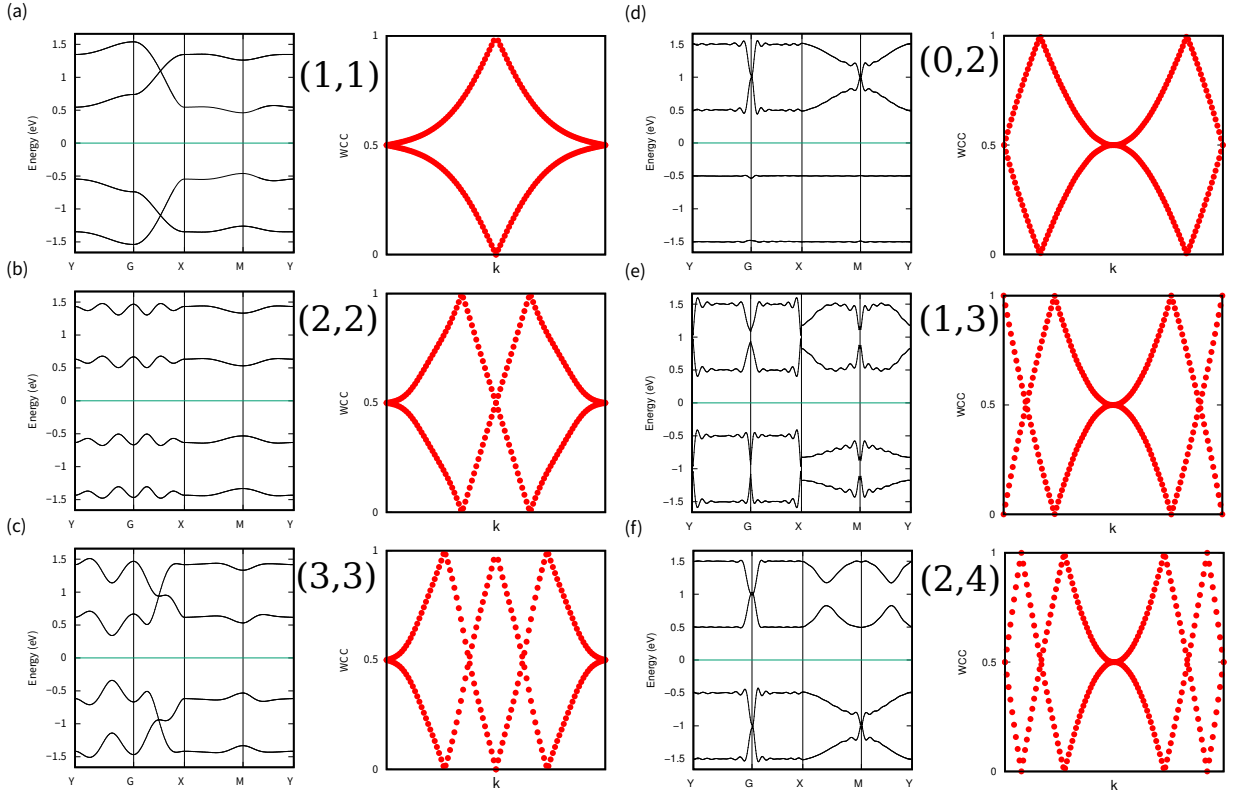


Figure 7. The band structure and two-band Wilson loops calculated of all Euler insulating phases studied in this work: (a-c) the balanced phases with $E_I = E_{II} = 1, 2, 3$, and (d-f) the imbalanced phases with $(E_I, E_{II}) = (0, 2), (1, 3)$ and $(2, 4)$.

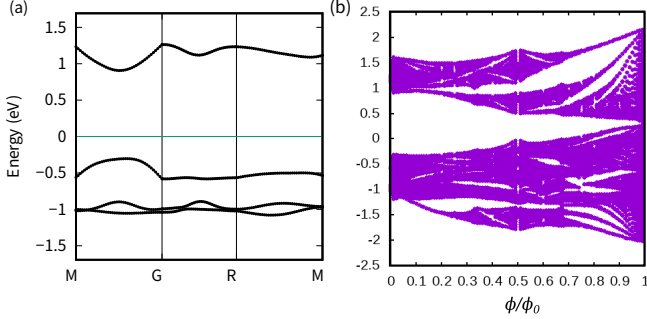


Figure 8. The band structure (a) and (b) Hofstadter butterfly in the case that one more band is in the occupied subspace for the $(E_I, E_{II}) = (2, 0)$ model.

tion $t_{ij} \rightarrow \tilde{t}_{ij} = t_{ij} \exp(i\phi_{ij})$ with $\phi_{ij} = (2\pi/\phi_0) \int_{\mathbf{R}_i}^{\mathbf{R}_j} \mathbf{A} \cdot d\mathbf{r}$ where, in the Landau gauge, the vector potential is $\mathbf{A} = (0, Bx)$ for $\mathbf{B} = B\hat{e}_z$, and $\phi_0 = 2\pi\hbar/e = h/e$ is the magnetic flux quantum. In our models, we assume well localized atomic orbitals and thus integrate the vector potential along direct paths, *i.e.* $\phi_{ij} \approx (\pi/\phi_0)[\mathbf{A}(\mathbf{R}_i) + \mathbf{A}(\mathbf{R}_j)] \cdot (\mathbf{R}_j - \mathbf{R}_i)$ [71], with \mathbf{A} defined within the periodic Landau gauge for lattice models [92]. Following the regular setups, we will restrict to the case when there is rational number of quantum flux per half unit cell, *i.e.* $\phi = \int_{\text{u.c.}} Bd^2\mathbf{r} = a_x a_y B = 2(p/q)\phi_0$ with

$p, q \in \mathbb{Z}$ and $\text{gcd}(p, q) = 1$, and $\{a_x, a_y\}$ the lengths of the primitive vectors in the x, y -directions. Labeling the x -component of atomic sites position as $\mathbf{R}_{i,x} = a_x n_i$ with $n_i \in \mathbb{Z}$, we for instance find $\phi_{i,i+1_y} = 2\pi n_i (p/q)$. While for $p/q = 1$ (*i.e.* $\phi = 2\phi_0$) we have $\tilde{t}_{ij} = t_{ij}$ and there is no effect of the magnetic field, when $p/q \neq 1$ we have the periodicity $\tilde{t}_{i+(q1_x), i+(q1_x)+1_y} = t_{i,i+1_y} \exp(i2\pi(n_i + q)(p/q)) = \tilde{t}_{i,i+1_y}$. We thus conclude under a rational magnetic field the tight-binding model is effectively described in terms of an enlarged magnetic unit cell containing q non-magnetic unit cells and defined through the primitive lattice vectors $\tilde{\mathbf{a}}_1 = q\mathbf{a}_1$ and $\tilde{\mathbf{a}}_2 = \mathbf{a}_2$.

We can now define the magnetic Bloch orbitals through

$$|\varphi_{(\alpha,m)}, \mathbf{k}\rangle \propto \sum_{\tilde{\mathbf{R}}} e^{i\mathbf{k} \cdot (\tilde{\mathbf{R}} + \mathbf{r}_\alpha + m\mathbf{a}_1)} |w_{(\alpha,m)}, \tilde{\mathbf{R}} + \mathbf{r}_\alpha + m\mathbf{a}_1\rangle, \quad (\text{H1})$$

and the magnetic Bloch Hamiltonian as

$$\mathcal{H} = \sum_{\alpha\beta, mm', \mathbf{k}} |\varphi_{(\alpha,m)}, \mathbf{k}\rangle H_{\alpha\beta, mm'}(\mathbf{k}) \langle \varphi_{(\beta,m')}, \mathbf{k}|, \quad (\text{H2})$$

where m is the sub-lattice degree of freedom that emerges from the reduced periodicity caused by finite rational magnetic field, *i.e.* for each orbital α of the non-magnetic system located at $\mathbf{R} + \mathbf{r}_\alpha$ within the non-magnetic unit cell centered at \mathbf{R} , the magnetic system has q orbitals

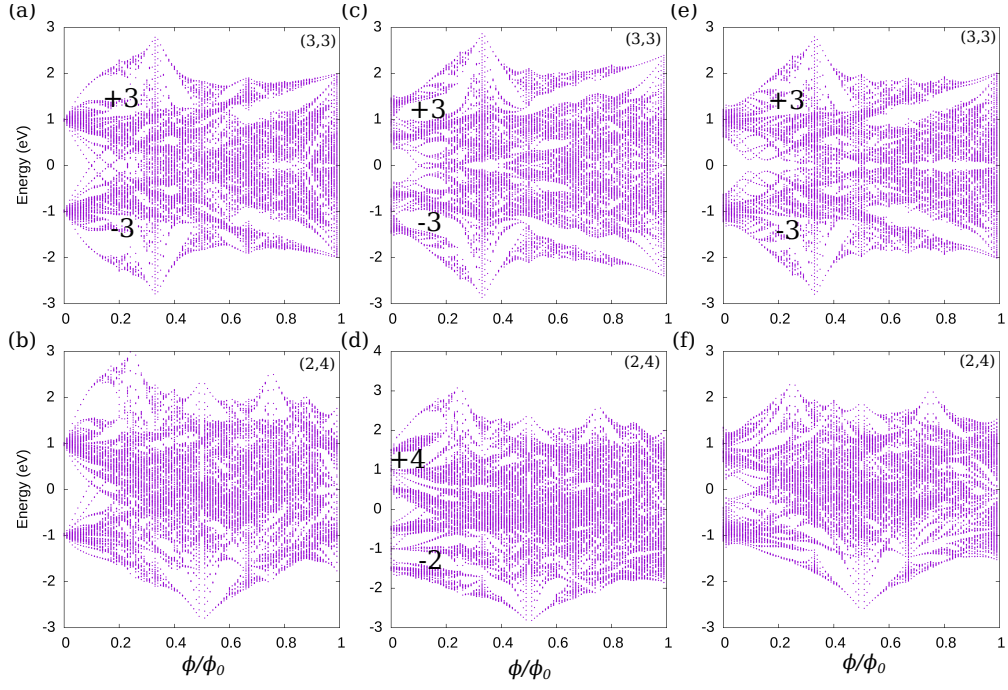


Figure 9. Hofstadter butterfly spectra for (a,c,e) the balanced phase $E_I = E_{II} = 3$, and (b,d,f) the imbalanced phase $(E_I, E_{II}) = (2, 4)$. Similarly to the main text, we successively consider (a,b) the flat-band limit with m_z symmetry, (c,d) the dispersive phases with the hidden symmetry ($h_{yy} = 0$), and (e,f) the dispersive phases that break the hidden symmetry.

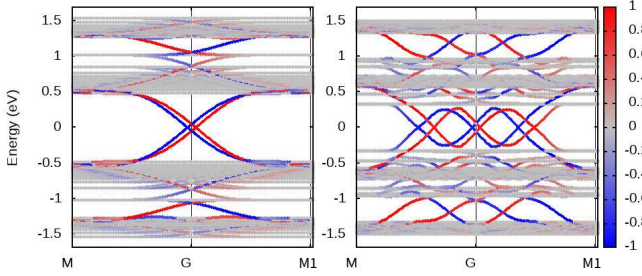


Figure 10. Energy spectrum at small magnetic flux of a finite system with open boundary condition, for the phases $(E_I, E_{II}) = (1, 1)$ (a) and $(3, 3)$ (b). The chiral edge branches (red for the left edge, blue for the right edge) indicates the Chern numbers at the corresponding energy gaps. The Chern numbers of the magnetic subgaps are bounded from below by the Euler classes.

$\{(\alpha, m)\}_{m=1, \dots, q}$ located at $\{\tilde{\mathbf{R}} + \mathbf{r}_\alpha + (m-1)\mathbf{a}_1\}_{m=1, \dots, q}$ within the magnetic unit cell centered at $\tilde{\mathbf{R}}$.

1. Example of a square lattice model with magnetic field

In this subsection we give the tight-binding Hamiltonian with nonzero magnetic field explicitly. For the sake of brevity, here we adapt the Landau gauge and assume all the orbitals are on the same position. The procedures

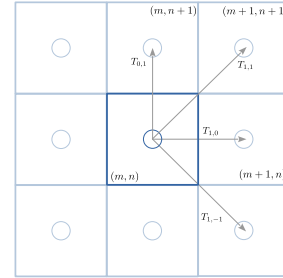


Figure 11. A diagram of the hopping $T_{i,j}$ in the square lattice. In 4-band models, each T_{ij} represents a 4 matrix of hopping integrals.

can easily be generalized with periodic Landau gauge.

The Landau gauge writes: $A(x, y) = (-By, 0)$ which satisfies $\nabla \times A = B$. With the Peierls substitution, the periodicity of the system is modified such that one needs to build a magnetic supercell. At a rational quantum flux $\phi = p/q\phi_0$, the magnetic supercell contains q unit cells.

Without the lost of generality, here we demonstrate the model with $\phi = 1/3\phi_0$ as an example. The magnetic unit cell is built with 3 replicas of the unit cell on the y direction

In the following process, we denote the hopping from the origin unit cell to unit cell (i, j) as T_{ij}^{xy} while xy are the orbital indices. The Hamiltonian without magnetic

field then writes :

$$\hat{H} = \sum_{i,j=-1}^1 e^{-ik \cdot (r_i, r_j)} T_{ij}$$

T_{ij} are hopping matrices between the orbits in i and j th unit cell, as shown in Fig. 11.

The gauge field A only acts on the x-direction component of the hoppings. With a magnetic field, the Peierls substitution calls for a gauge term. T_{ij} hoppings from unit cell (m, n) to $(m+i, n+j)$ picks up a phase

$$\phi = \int_{(m,n)}^{(m+i,n+j)} A \cdot dr = -Bi \cdot (2n+1)/2$$

assuming the straight-line Peierls paths.

As an example, in Fig. 12, we show the case of $\phi = 1/3\phi_0$ for the construction of magnetic supercells and the phases assigned to the hoppings. According to the Landau gauge, the $A = (-By, 0)$ field term extends the periodicity on y direction. At $\phi = 1/3\phi_0$, the magnetic supercell contains 3 lattice unit cells.

The Hamiltonian then expands to the magnetic supercells

$$\begin{aligned} H_{mag} = & \begin{pmatrix} T_{0,0} & 0 & 0 \\ 0 & T_{0,0} & 0 \\ 0 & 0 & T_{0,0} \end{pmatrix} \\ & + \begin{pmatrix} T_{1,0} & 0 & 0 \\ 0 & e^{2\pi i/3} T_{1,0} & 0 \\ 0 & 0 & e^{4\pi i/3} T_{1,0} \end{pmatrix} e^{-ik \cdot (r_x, 0)} \\ & + \begin{pmatrix} T_{-1,0} & 0 & 0 \\ 0 & e^{-2\pi i/3} T_{-1,0} & 0 \\ 0 & 0 & e^{-4\pi i/3} T_{-1,0} \end{pmatrix} e^{-ik \cdot (-r_x, 0)} \\ & + \begin{pmatrix} 0 & T_{0,1} & 0 \\ 0 & 0 & T_{0,1} \\ 0 & 0 & 0 \end{pmatrix} e^{-ik \cdot (0, r_y)} \\ & + \begin{pmatrix} 0 & 0 & 0 \\ T_{0,-1} & 0 & 0 \\ 0 & T_{0,-1} & 0 \end{pmatrix} e^{-ik \cdot (0, -r_y)} \\ & + \begin{pmatrix} 0 & 0 & 0 \\ e^{-\pi i/3} T_{-1,-1} & 0 & 0 \\ 0 & e^{3\pi i/3} T_{-1,-1} & 0 \end{pmatrix} e^{-ik \cdot (-r_x, -r_y)} \\ & + \begin{pmatrix} 0 & 0 & 0 \\ e^{\pi i/3} T_{1,-1} & 0 & 0 \\ 0 & e^{3\pi i/3} T_{1,-1} & 0 \end{pmatrix} e^{-ik \cdot (r_x, -r_y)} \\ & + \begin{pmatrix} 0 & e^{\pi i/3} T_{1,1} & 0 \\ 0 & 0 & e^{3\pi i/3} T_{1,1} \\ 0 & 0 & 0 \end{pmatrix} e^{-ik \cdot (r_x, r_y)} \\ & + \begin{pmatrix} 0 & e^{-\pi i/3} T_{-1,1} & 0 \\ 0 & 0 & e^{-3\pi i/3} T_{-1,1} \\ 0 & 0 & 0 \end{pmatrix} e^{-ik \cdot (-r_x, r_y)} \end{aligned}$$

Where $T_{i,j}$ are the hopping matrices corresponding to the orbitals.

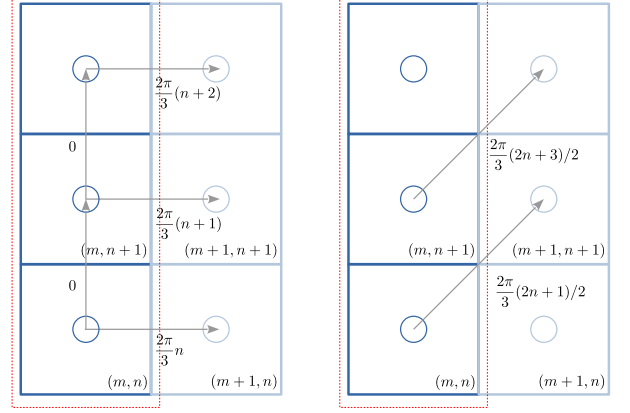


Figure 12. A diagram of phase terms at $\phi = 1/3\phi_0$. As indicated in the red dashed line, the magnetic supercell is composed of 3 unit cells to ensure periodicity. The phase terms is calculated with Peierls substitution assuming that the hopping is along a straight line.

Appendix I: The orbital magnetic moment of the complexified bands.

Near $B = 0$, the perturbative response to a magnetic field writes (neglecting the spins):

$$E = E_0(k) + m(k)B$$

Here $m(k)$ is the orbital magnetization, which describes the susceptibility of energy bands to a magnetic field. Its expression writes:

$$m = -\mu_B \frac{2m_e}{\hbar^2} \Im \sum_{l \neq n} \frac{\langle n | \partial_{k_x} H | l \rangle \langle l | \partial_{k_y} H | n \rangle}{E_{n,k} - E_{l,k}}$$

It can be observed from its formula that the orbital magnetization is closely related to the Berry phase. In flat-band Euler insulators, the orbital magnetization of the real eigenstates is exactly zero, while for complexified bands it is $\pm Eu$. Such a limit gives a closer look at the small magnetic field regimes.

On the other hand, in dispersive bands the orbital magnetization can still affect the spectrum but it does not dominate the energy levels. In dispersive bands, the difference of $H(k)$ itself would be much larger than the $m(k)B$ terms, which overrides the effect.

Appendix J: Three-band models

In general, the minimal number of total bands to have an Euler class in the occupied subspace is 3: there is only one conduction band which is not occupied. Due to the requirement of the overall Bloch conditions, the 3-band models can only show even Euler classes.

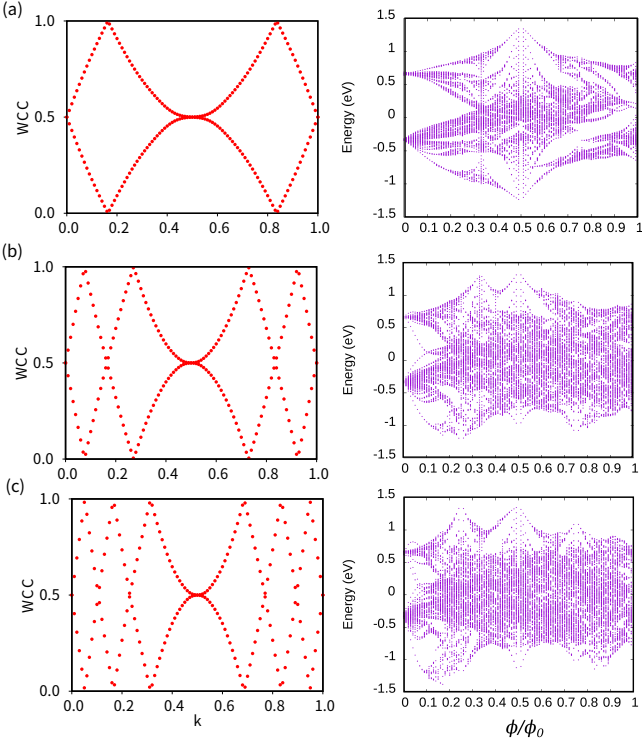


Figure 13. The Wilson loop and Hofstadter butterfly for flat 3-band models with (a) Euler number $E=2$ (b) $E=4$ (c) $E=6$ with the occupied 2-band subspace. The $E = n$ Wilson loop show a pair of winding $2n$.

In addition to the 4-band models shown in the main text, we have also calculated the Hofstadter butterflies of the 3-band models. In Figure.13, and Fig.14, the Wilson loop plots and the corresponding Hofstadter butterfly are presented for both degenerated (flat) bands and dispersive bands. The bandgap closing behavior is observed, similar as the 4-band Euler insulator case. In both flat and dispersive cases, the gap-closing flux decreases at larger Euler classes. However, the exact m_z limit is absent in 3-band models. In the 3-band case, the only interpretation is through the Chern-rotation approach, which predicts the response of Euler bands as a pair of Chern bands. It also works well in explaining the trend of gap-closing flux.

Appendix K: Peierls paths and the periodicity of Hofstadter butterfly

To consider the periodicity of the Hofstadter butterfly, we start from a general form of tight-binding model where

$$\hat{H} = \sum t_{ij} c_i^\dagger c_j$$

The operators c_i^\dagger or c_i create or annihilate a state on site i . t_{ij} indicates the hopping integral between orbitals i and

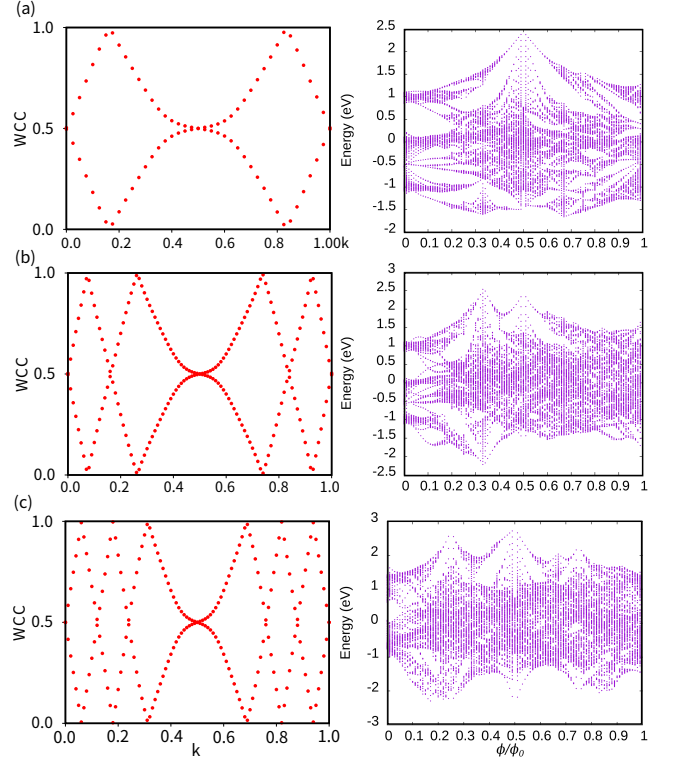


Figure 14. The Wilson loops and corresponding Hofstadter plots for 3-band models with finite dispersion. (a) Euler number $E=2$ (b) $E=4$ and (c) $E=6$.

j . With a finite magnetic field, the Peierls substitution gives a phase modulation: $t_{ij} \rightarrow e^{i\phi_{ij}} t_{ij}$.

In the most general case, one should have different loops formed by the Peierls paths. The Hamiltonian returns to the same eigenvalue up to a gauge transformation: $\hat{H} \sim G^\dagger \hat{H} G$. Such a condition requires the flux quanta of all the loops be multiplies of 2π . To determine the periodicity of Hofstadter butterfly, it then needs to find the series of areas of the loops.

Such a problem of calculating the loops is related to the lattice structures, and consequently, the space groups. In the following derivations, we list the cases and discuss the periodicity of the Hofstadter spectrum.

There is a simple case to present: in the unit of lattice vectors, all the sites are on rational positions: $r_i = \frac{p}{q}$. The denominator q does not have to be the same since we can multiply different qs .

In number theory, there is a theorem sometimes referred as Bézout's theorem :

For two integer numbers p, q the equation holds:

$$px + qy = N \times \text{gcd}(p, q)$$

since the expression of areas can be written as:

$$A = \begin{vmatrix} a & b \\ c & d \end{vmatrix}$$

which is in the same form, the series of loop areas is then determined by the series of rational site positions.

However, in a general case where one may have irra-

tional site positions, the Bezout method does not hold and the Hofstadter butterfly can never repeat itself exactly.